

University of Kentucky

UKnowledge

---

Theses and Dissertations--Earth and  
Environmental Sciences

Earth and Environmental Sciences

---


2023

## DISCOVERY OF THE MIDDLE MANTLE TRANSITION ZONE (MMTZ) AND ITS GEODYNAMIC SIGNIFICANCE

Yuping Wang

University of Kentucky, yupingwanggeo@gmail.com

Author ORCID Identifier:

 <https://orcid.org/0009-0001-2246-5955>

Digital Object Identifier: <https://doi.org/10.13023/etd.2023.464>

[Right click to open a feedback form in a new tab to let us know how this document benefits you.](#)

### Recommended Citation

Wang, Yuping, "DISCOVERY OF THE MIDDLE MANTLE TRANSITION ZONE (MMTZ) AND ITS GEODYNAMIC SIGNIFICANCE" (2023). *Theses and Dissertations--Earth and Environmental Sciences*. 104.  
[https://uknowledge.uky.edu/ees\\_etds/104](https://uknowledge.uky.edu/ees_etds/104)

This Master's Thesis is brought to you for free and open access by the Earth and Environmental Sciences at UKnowledge. It has been accepted for inclusion in Theses and Dissertations--Earth and Environmental Sciences by an authorized administrator of UKnowledge. For more information, please contact [UKnowledge@lsv.uky.edu](mailto:UKnowledge@lsv.uky.edu).

## **STUDENT AGREEMENT:**

I represent that my thesis or dissertation and abstract are my original work. Proper attribution has been given to all outside sources. I understand that I am solely responsible for obtaining any needed copyright permissions. I have obtained needed written permission statement(s) from the owner(s) of each third-party copyrighted matter to be included in my work, allowing electronic distribution (if such use is not permitted by the fair use doctrine) which will be submitted to UKnowledge as Additional File.

I hereby grant to The University of Kentucky and its agents the irrevocable, non-exclusive, and royalty-free license to archive and make accessible my work in whole or in part in all forms of media, now or hereafter known. I agree that the document mentioned above may be made available immediately for worldwide access unless an embargo applies.

I retain all other ownership rights to the copyright of my work. I also retain the right to use in future works (such as articles or books) all or part of my work. I understand that I am free to register the copyright to my work.

## **REVIEW, APPROVAL AND ACCEPTANCE**

The document mentioned above has been reviewed and accepted by the student's advisor, on behalf of the advisory committee, and by the Director of Graduate Studies (DGS), on behalf of the program; we verify that this is the final, approved version of the student's thesis including all changes required by the advisory committee. The undersigned agree to abide by the statements above.

Yuping Wang, Student

Dr. Keely A. O'Farrell, Major Professor

Dr. Kevin M. Yeager, Director of Graduate Studies

DISCOVERY OF THE MIDDLE MANTLE TRANSITION ZONE (MMTZ) AND ITS  
GEODYNAMIC SIGNIFICANCE

---

THESIS

---

A thesis submitted in partial fulfillment of the  
requirements for the degree of Master of Science in the  
College of Arts and Sciences  
at the University of Kentucky

By

Yuping Wang

Lexington, Kentucky

Director: Dr. Keely A. O'Farrell, Professor of Geophysics and Geodynamics

Lexington, Kentucky

2023

Copyright © Yuping Wang 2023  
<https://orcid.org/0009-0001-2246-5955>

## ABSTRACT OF THESIS

### DISCOVERY OF THE MIDDLE MANTLE TRANSITION ZONE (MMTZ) AND ITS GEODYNAMIC SIGNIFICANCE

Global mantle discontinuities and mantle transition zones are crucial to the earth's evolution. By employing K-Means clustering, which belongs to cluster analysis in machine learning (ML), on shear velocity variation data, we generate heterogeneity percentage profiles for three different global tomographic models (Models S362WMANI+M, SEMUCB-WM1, and S40RTS). Key cluster percentage shifts, which are observed at around 400 km, 650 km, 1050 km, 1500 km, and 2700 km, suggest global mantle discontinuities at corresponding depths. All profiles also indicate a global discontinuity in the lower mantle between 2200 km and 2600 km. The middle mantle transition zone (MMTZ), bounded between 1050 km and 1500 km discontinuities, is detected for the first time. Mantle convection modeling with the global geoid is conducted using the HC code to demonstrate the viscosity jump in this new MMTZ.

**KEYWORDS:** global tomographic model, K-Means clustering, mantle convection modeling, middle mantle transition zone (MMTZ), viscosity jump

Yuping Wang

---

Name of Student

09/20/2023

---

Date

DISCOVERY OF THE MIDDLE MANTLE TRANSITION ZONE (MMTZ) AND ITS  
GEODYNAMIC SIGNIFICANCE

By  
Yuping Wang

Dr. Keely A. O'Farrell

---

Director of Thesis

Dr. Kevin M. Yeager

---

Director of Graduate Studies

09/20/2023

---

Date

## DEDICATION

In memory of Alfred Wegener (1880–1930), the originator of continental drift.  
He enlightened me about this research in my dream.

## ACKNOWLEDGMENTS

I would like to express my deepest appreciation to Dr. Keely A. O'Farrell. As my supervisor and chair of my thesis committee, she guided me into the world of mantle convection modeling. Her invaluable patience is what I admire most. Many thanks to Dr. J. Ryan Thigpen and Dr. Edward W. Woolery, who are members of the thesis committee. Dr. J. Ryan Thigpen allowed me to use the workstation in his laboratory for numerical simulation. Dr. Edward W. Woolery helped me settle down in Lexington and organized the seismic field trip. I am also grateful to scholars who are willing to share their seismic models and modeling codes with the public.

I appreciate the conversation with Alfred Wegener in my dream. He reminded me to look at the global map in "a vertical way". This enlightened me about dividing shear velocity into two groups and using heterogeneity percentage profiles to deduce global discontinuities in the mantle.

I am also thankful to my family, mostly my spouse and parents. Their consistent encouragement and support are indispensable in the process of finishing this degree.

## TABLE OF CONTENTS

ACKNOWLEDGMENTS .....	iii
TABLE OF CONTENTS .....	iv
LIST OF TABLES .....	vi
LIST OF FIGURES.....	vii
CHAPTER 1. INTRODUCTION .....	1
1.1 Continental drift, seafloor spreading, and plate tectonics.....	1
1.2 Mantle dynamics and numerical simulation .....	1
1.3 Global geoid and mantle viscosity .....	2
1.4 PREM and mantle discontinuities.....	3
1.4.1 Preliminary reference earth model (PREM) .....	3
1.4.2 400 km and 650 km discontinuities .....	3
1.4.3 1050 km discontinuity.....	4
1.4.4 D'' discontinuity .....	4
1.5 Phase transitions of mantle minerals.....	4
1.6 Machine learning in geophysics.....	5
CHAPTER 2. METHODS .....	7
2.1 From the earth's surface to the mantle.....	7
2.2 Synthesis of heterogeneity percentage profiles.....	7
2.2.1 Shear velocity models .....	8
2.2.2 Extraction of seismic data .....	9
2.2.3 K-Means clustering method.....	11
2.2.4 Heterogeneity percentage profiles .....	12
2.3 Mantle convection modeling.....	13
2.3.1 Governing equations .....	13
2.3.2 Tomography and the mantle's density structure.....	14
2.3.3 The mantle's layer model and reference geoid.....	15
CHAPTER 3. RESULTS .....	17
3.1 Seismic data and clustering results .....	17
3.2 Spectrum amplitude charts.....	18
3.3 Global cluster maps and global shear velocity variation maps.....	18



3.4 Cluster center charts.....	19
3.5 Heterogeneity percentage profiles .....	20
3.5.1 Data types and reference models .....	20
3.5.2 Geophysical significance of abrupt cluster percentage shifts .....	21
3.5.3 Global mantle discontinuities inferred from key cluster percentage shifts... ..	21
3.5.4 Other discontinuities in the mantle .....	23
3.6 Modeled geoid maps.....	23
CHAPTER 4. DISCUSSION.....	46
4.1 Reliability analysis of inferred global mantle discontinuities.....	46
4.2 Global discontinuities in the mantle .....	46
4.2.1 400 km, 650 km, and 2700 km discontinuities .....	47
4.2.2 1050 km and 1500 km discontinuities .....	47
4.3 Transition zones in the mantle .....	49
4.3.1 Upper mantle transition zone (UMTZ).....	49
4.3.2 Middle mantle transition zone (MMTZ).....	49
4.4 Viscosity jump in MMTZ and its geodynamical significance.....	49
CHAPTER 5. CONCLUSION.....	51
REFERENCES .....	52
VITA.....	59

## LIST OF TABLES

Table 2.1 Combinations of viscosity ratios for the mantle's layer model. ....	16
Table 3.1 Correlation results for modeling with different viscosity ratio combinations. .	24

## LIST OF FIGURES

Figure 1.1 Shear velocity profile for isotropic PREM.....	6
Figure 3.1 Spectrum amplitude chart for Model S362WMANI+M. ....	25
Figure 3.2 Spectrum amplitude chart for Model S40RTS. ....	26
Figure 3.3 Spectrum amplitude chart for Model SEMUCB-WM1.....	27
Figure 3.4 Global cluster maps and global shear velocity variation maps for Model S362WMANI+M. ....	28
Figure 3.5 Global cluster maps and global shear velocity variation maps for Model S40RTS. ....	29
Figure 3.6 Global cluster maps and global shear velocity variation maps for Model SEMUCB-WM1. ....	30
Figure 3.7 Cluster center chart for Model S362WMANI+M. ....	31
Figure 3.8 Cluster center chart for Model S40RTS. ....	32
Figure 3.9 Cluster center chart for Model SEMUCB-WM1.....	33
Figure 3.10 Cluster center profiles and heterogeneity percentage profiles for Model S362ANI+M. ....	34
Figure 3.11 Cluster center profiles and heterogeneity percentage profiles for Model SEMUCB-WM1. ....	35
Figure 3.12 Global cluster maps at degree 60 for all three seismic models. ....	36
Figure 3.13 Heterogeneity percentage profiles at degrees 20 and 60 for Model S362WMANI+M. ....	37
Figure 3.14 Heterogeneity percentage profiles at degrees 35 and 60 for Model S40RTS. ....	38
Figure 3.15 Heterogeneity percentage profiles at degrees 40 and 60 for Model SEMUCB-WM1. ....	39
Figure 3.16 Heterogeneity percentage profiles at degree 60 for Model S362WMANI+M. ....	40
Figure 3.17 Heterogeneity percentage profiles at degree 60 for Model S40RTS.....	41
Figure 3.18 Heterogeneity percentage profiles at degree 60 for Model SEMUCB-WM1. ....	42
Figure 3.19 Modeled geoid map for Case 1.....	43
Figure 3.20 Modeled geoid map for Case 2.....	44
Figure 3.21 Modeled geoid map for Case 3.....	45

## CHAPTER 1. INTRODUCTION

Considerable research attention has been devoted to the structure of the deep mantle. This thesis is based on research using the K-Means clustering method to identify global mantle discontinuities. The thesis is divided into five chapters. Chapter one provides the necessary background information. Chapter two details the methods used in the study. Research results are listed in chapter three. In chapter four, we discuss the results and their scientific implications. Chapter five serves as the summary of this thesis.

### 1.1 Continental drift, seafloor spreading, and plate tectonics

It is generally agreed that plate tectonics is a major achievement in modern geoscience. In his seminal discussion of the origin of continents and oceans, Wegener proposed the hypothesis of continental drift (Wilson, 1963; Wegener, 1966). The most criticized issue of this hypothesis, the driving mechanism, was successfully resolved by Holmes with thermal convection of the mantle (Holmes, 1931). Hess and Dietz discovered seafloor spreading during their studies of ocean basins (Dietz, 1961; Hess, 1962). Around the same time, Wilson used the concept of hotspots to explain the formation of the Hawaiian Islands and other similar island chains (Wilson, 1963; Wilson, 1965). After these astonishing discoveries, Le Pichon built a model to include continental drift and seafloor spreading (Le Pichon, 1968). Morgan proposed the mantle plume theory and used it to explain the formation of island chains (Morgan, 1971). Moreover, he linked plate movements to plumes in mantle convection (Morgan, 1972).

### 1.2 Mantle dynamics and numerical simulation

Because of the importance of mantle convection to the theory of plate tectonics, mantle dynamics has been developed accordingly. Due to the inaccessibility of the mantle,

numerical simulation plays an important role in these studies. With numerical modeling, numerous scholars have investigated the implications of mantle dynamics. Turcotte and Oxburgh developed the first numerical model of mantle convection to explain continental drift (Turcotte, 1967). Hager and O'Connell constructed a simple global model to describe plate dynamics and mantle convection (Hager & O'Connell, 1981). The HC code for this model has been widely deployed to explore different issues about the mantle (e.g., Davies, Stegman, & Dumberry, 2014; Wang, Holt, & Ghosh, 2015; Rudolph, Moulik, & Lekić, 2020).

In recent decades, due to advances in computer science, several software packages have been developed to facilitate high-resolution modeling of mantle convection (e.g., Zhong, Zuber, Moresi, & Gurnis, 2000; Tackley, 2008; Kronbichler, Heister, & Bangerth, 2012; Heister, Dannberg, Gassmöller, & Bangerth, 2017). These software packages have been implemented to investigate mantle dynamics and earth processes (e.g., Stadler, et al., 2010; Mao & Zhong, 2018; Davies, et al., 2019).

### 1.3 Global geoid and mantle viscosity

Research has shown that the global geoid is governed by the mantle. Specifically, it is controlled by both the mantle's density structure and changing topographies (Hager, Clayton, Richards, Comer, & Dziewonski, 1985; Ricard, Richards, Lithgow-Bertelloni, & Le Stunff, 1993). Dynamic topographies caused by mantle flow are dependent on viscosity changes in the mantle. When the structure of the mantle's density is known, it is feasible to use the global geoid to constrain the structure of the mantle's viscosity.

By conducting mantle convection modeling with the global geoid, scholars have investigated viscosity variations in the mantle (e.g., Thoraval & Richards, 1997; Zhong &

Davies, 1999; Liu & Zhong, 2016). Simulation results show that changes in the mantle's radial viscosity are the main cause of long-wavelength geoid anomalies (Richards & Hager, 1984; Hager & Richards, 1989; Liu & Zhong, 2015). Lateral viscosity variations in the mantle, according to modeling results, have little effect on the geoid (Richards & Hager, 1989; Moucha, Forte, Mitrovica, & Daradich, 2007; Ghosh, Becker, & Zhong, 2010).

#### 1.4 PREM and mantle discontinuities

##### 1.4.1 Preliminary reference earth model (PREM)

The preliminary reference earth model (PREM), derived from seismic data, is the most popular 1D global model depicting the structure of the earth (Dziewonski & Anderson, 1981). This model has been extensively employed as the reference model in geophysical studies (e.g., Ritsema, Deuss, Van Heijst, & Woodhouse, 2011; Zeng, Sasselov, & Jacobsen, 2016). As shown in Figure 1.1, PREM includes six discontinuities in the mantle (400 to 2891 km). The algorithm for calculating shear velocities at different depths in isotropic PREM is available on GitHub<sup>1</sup>. It is noteworthy that not all six mantle discontinuities in PREM have been acknowledged as global discontinuities. PREM also does not include all global discontinuities in the mantle.

##### 1.4.2 400 km and 650 km discontinuities

Two discontinuities around 400 km and 650 km depths have been studied comprehensively by researchers (e.g., Niazi & Anderson, 1965; Richards & Wicks Jr, 1990; Simmons & Gurrola, 2000; Ai & Zheng, 2003). In PREM, they are located at 400 km and 670 km separately. Even though these two discontinuities have different topographies (Schmerr & Garnero, 2007; Cottaar & Deuss, 2016; Wu, Ni, & Irving, 2019),

---

<sup>1</sup><https://github.com/andreww/prem4derg>

it is confirmed that their depth difference (i.e., thickness of the upper mantle transition zone) is between 220 and 260 km (Gurrola & Minster, 1998; Gu & Dziewonski, 2002; Burky, Irving, & Simons, 2023).

#### 1.4.3 1050 km discontinuity

1050 km discontinuity is not included in PREM. However, it has been observed in recent research. In their investigation of the Tonga subduction zone, Kawakatsu and Niu originally reported this discontinuity as a "920 km discontinuity" (Kawakatsu & Niu, 1994). Then, they discovered that the depth of discontinuity varies between 900 and 1080 km beneath different subduction zones (Niu & Kawakatsu, 1997). In Zhang's research, this discontinuity was observed underneath the central Pacific at around 1000 km (Zhang, Irving, Simons, & Alkhalifah, 2023). The global shear velocity pattern change at around 1000 km also indicates the existence of a seismic discontinuity (Durand, Debayle, Ricard, Zaroli, & Lambotte, 2017).

#### 1.4.4 D'' discontinuity

D'' discontinuity, marked by an increase in seismic velocity near the core mantle boundary (CMB), has been detected around 250–270 km above CMB (Wyssession, et al., 1998; He & Wen, 2011). However, the D'' discontinuity is not included in PREM. Instead, PREM contains a discontinuity at 2741 km.

#### 1.5 Phase transitions of mantle minerals

In general, phase transitions of minerals in the mantle can explain 400 km, 650 km, and D'' discontinuities. 400 km and 660 km discontinuities are attributed to phase changes in the mineral systems of olivine and pyroxenes (Ringwood, 1969; Shim, Duffy, & Shen, 2001). D'' discontinuity results from the transition of perovskite to post-perovskite

(Murakami, Hirose, Kawamura, Sata, & Ohishi, 2004; Iitaka, Hirose, Kawamura, & Murakami, 2004).

Not all discontinuities are explicable by major phase changes. For example, a 1050 km discontinuity has been discovered underneath both subduction and non-subduction areas, but no phase transitions have been reported from high-pressure experiments of major mineral components of the lower mantle under similar conditions (Fiquet, Dewaele, Andrault, Kunz, & Le Bihan, 2000; Shim, Duffy, & Shen, 2000; Irifune & Tsuchiya, 2015).

## 1.6 Machine learning in geophysics

Machine learning (ML) may lead to significant discoveries in solid earth geoscience (Bergen, Johnson, de Hoop, & Beroza, 2019). In geophysics, it has been used to investigate well-known issues such as earthquake prediction (Rouet-Leduc, et al., 2017) and electron transfer in minerals (Li, et al., 2023). In seismic studies of the mantle, cluster analysis has been utilized to find patterns in seismic data. In developing velocity models, waveforms were grouped based on their similarity (Houser, Masters, Shearer, & Laske, 2008). To recognize features of the mantle, cluster analysis was applied to mantle tomographic models (Lekic & Romanowicz, 2011; Lekic, Cottaar, Dziewonski, & Romanowicz, 2012; Cottaar & Lekic, 2016). In this study, the K-Means clustering method is used to identify discontinuities in the mantle.



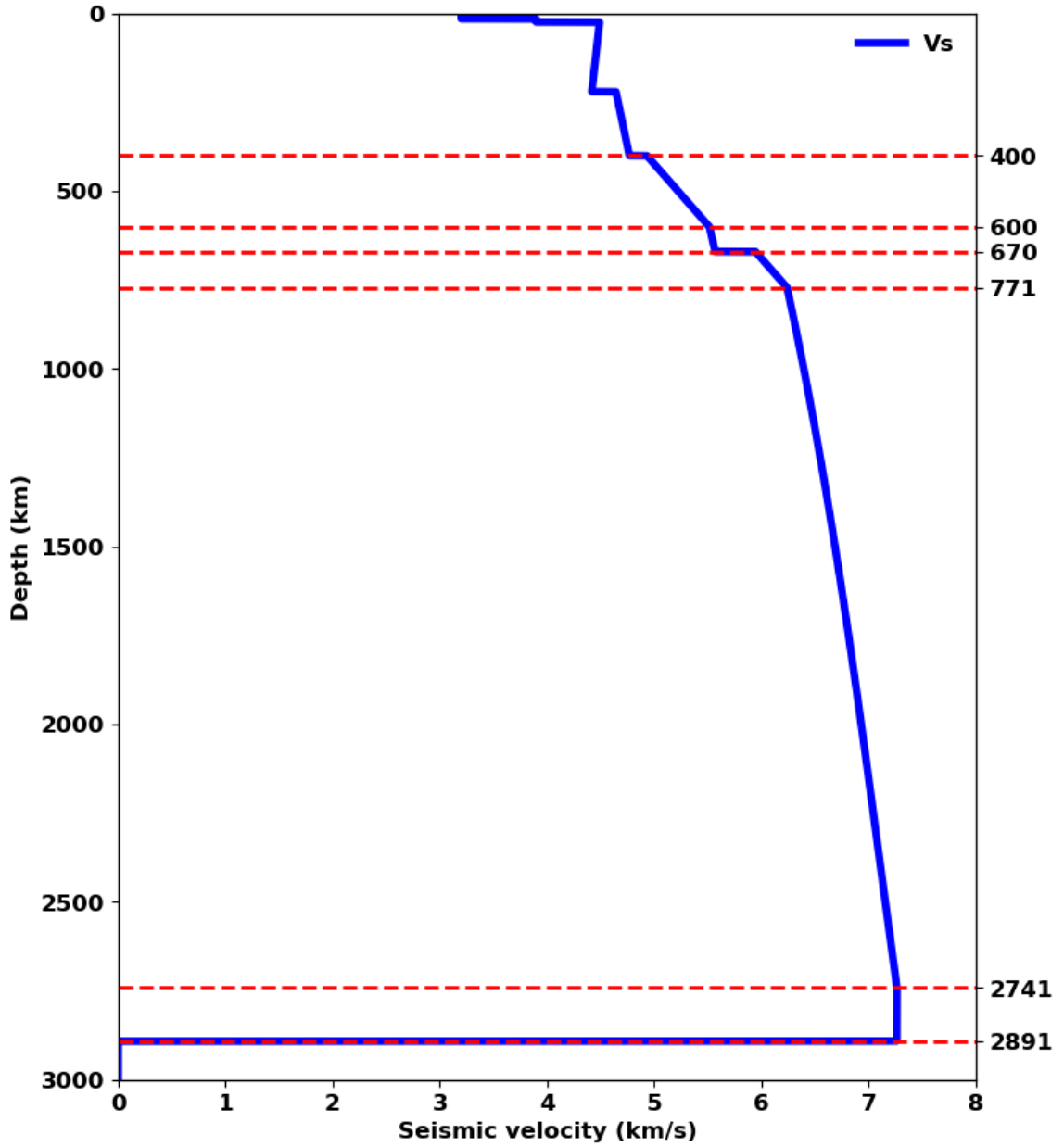


Figure 1.1 Shear velocity profile for isotropic PREM. Discontinuities in the mantle (400 to 2891 km) are denoted by red dashed lines.

## CHAPTER 2. METHODS

### 2.1 From the earth's surface to the mantle

The earth's surface can be divided into two distinct components: land and ocean. Similarly, in the mantle, seismic velocity can be grouped into two separate clusters (a high velocity cluster and a low velocity cluster). For either cluster, its percentage changes with depth. Abrupt shifts in cluster percentage represent seismic discontinuities. After synthesizing the cluster percentage profile, we can recognize abrupt shifts and then infer discontinuities in the deep earth.

For a seismic model, an abrupt shift in its cluster percentage profile indicates a discontinuity. However, due to the model's intrinsic bias, the shift correlated to a discontinuity may not be conspicuous. In other words, abrupt shifts, which are recognized in the cluster percentage profile of one model, may not denote all seismic discontinuities. This research uses shear velocity models to identify global discontinuities in the mantle. Because shear velocity variations in the mantle essentially reflect the mantle's heterogeneity, the depth profile of cluster percentage is referred to as the "heterogeneity percentage profile" in this thesis.

### 2.2 Synthesis of heterogeneity percentage profiles

In this research, it takes three steps to synthesize the heterogeneity percentage profile for a seismic model. First, seismic data (both shear velocity variation data and spectrum amplitude data) are extracted for the seismic model. Shear velocity variation data is then grouped into two separate clusters (a high velocity cluster and a low velocity cluster) using cluster analysis. At last, after choosing one cluster, its percentages are calculated and then combined along depth to generate the model's heterogeneity percentage profile.

For the reliability of heterogeneity percentage profiles, it is important to ensure that clusters are accurate. Clusters must be consistent over depth and degree ranges. For the purpose of deducing discontinuities from profiles, seismic models must be stable when their heterogeneity percentage profiles are constructed.

### 2.2.1 Shear velocity models

The main objective of this research is to identify global mantle discontinuities using shear velocity models. Diverse seismic models are required to avoid the bias of a specific model. To verify the stability of seismic models, they need to be expressed in spherical harmonics. For a seismic model, if its spectra are flat at some depths, aliasing can be created when it is truncated at low degrees (Su, Woodward, & Dziewonski, 1994). Seismic models for this study must be sufficiently detailed (i.e., have components of high harmonic degrees). With consideration of these requirements, we chose three global tomography models. Multiple distinctions exist between Models S362WMANI+M, SEMUCB-WM1, and S40RTS, which are explained below.

For Model S362WMANI+M, it is created with four types of seismic data: normal modes, body waves, surface waves, and long-period waveforms. Inversion is conducted using ray theory. For creating the model, the crustal model of Model CRUST2.0 and the 1-D reference model of Model STW105 are used. This model has a full spectral range up to degree 24. Model S362WMANI+M is distinguished by its inclusion and exploitation of new mode-splitting data (Moulik & Ekström, 2014).

For Model SEMUCB-WM1, it is produced using waveform data. Inversion is performed via a hybrid full-waveform inversion method, a combination of SEM and NACT approaches. For producing the model, Model CRUST2.0 and a custom model are used as

the crustal model and 1-D reference model, respectively. This model has a full spectral range up to degree 96. Different from Models SEMum and SEMum2, Model SEMUCB-WM1 is the first model for the whole mantle built with the same method (French & Romanowicz, 2014).

For Model S40RTS, it is developed with three types of seismic data: Rayleigh wave phase velocity, teleseismic traveltimes, and normal-mode splitting function. Inversion is completed using ray theory. For developing the model, the crustal model of Model CRUST2.0 and the 1-D reference model of PREM are used. This model has a full spectral range up to degree 40. Compared to the preceding Model S20RTS, a much larger dataset is used to build Model S40RTS (Ritsema, Deuss, Van Heijst, & Woodhouse, 2011).

When comparing these three seismic models, the most noticeable difference is that they are built with distinct types of datasets. Two different inversion methods, ray theory and waveform inversion, are applied to create models. Three seismic models are constructed with different reference models. As for similarities between models, all models are for the whole mantle and corrected with the same crustal model, Model CRUST2.0. All three models are global mantle models and contain high harmonic degree components when expressed in spherical harmonics.

### 2.2.2 Extraction of seismic data

A Python tool called SeisTomoPy was developed to help extract, process, and analyze global mantle tomographic models (Durand, Abreu, & Thomas, 2018). This tool includes seismic models that can be expressed in spherical harmonics. It supports the extraction of various seismic-related data up to degree 60. The upper limits of spectral ranges for Models S362WMANI+M, SEMUCB-WM1, and S40RTS are degrees 24, 96,

and 40, respectively. In this research, for recognizing global discontinuities in the mantle, seismic data up to degree 60 is adequate.

There are a number of advantages to using SeisTomoPy. First, it contains all three seismic models picked for this research. Moreover, shear velocity variations are expressed in spherical harmonics and can be extracted up to degree 60. We can infer discontinuities from heterogeneity percentage profiles at degree 60. For each seismic model, by comparing its heterogeneity percentage profiles at a low degree and degree 60, we can verify the model's stability at degree 60. Moreover, we can also obtain spectrum amplitude data with SeisTomoPy.

In this research, we use SeisTomoPy to extract seismic data, both shear velocity variation data and spectrum amplitude data, for all three models. The spectrum amplitude of shear velocity  $V_s$  is defined as:

$$S = \sqrt{\frac{1}{4\pi} \sum_{m=-l}^l \left( \frac{dV_s}{V_s}(z) \right)_{lm} \left( \frac{dV_s}{V_s}(z) \right)_{lm}^*} \quad \text{Equation 2.1}$$

where  $\left( \frac{dV_s}{V_s}(z) \right)_{lm}$  represents the spherical harmonic coefficients of  $V_s$  at depth  $z$  and degree  $l$ . The asterisk stands for the corresponding complex conjugate.

Both shear velocity variation data and spectrum amplitude data are important for this research. Shear velocity variation data is used to produce global shear velocity variation maps and heterogeneity percentage profiles. We can use global shear velocity variation maps to verify the accuracy of clusters. Discontinuities in the mantle are inferred

from heterogeneity percentage profiles. Spectrum amplitude data is used to generate spectrum amplitude charts. We can use spectrum amplitude charts to evaluate the adequacy of extracting seismic data up to degree 60.

### 2.2.3 K-Means clustering method

Cluster analysis, also called clustering, belongs to unsupervised machine learning (ML). Different clustering methods (e.g., BIRCH, DBSCAN, and K-Means) are widely used in a variety of fields. These methods are effective at uncovering patterns in data that cannot be discovered using conventional methods. Clustering methods are included in different Python libraries, such as SciPy and scikit-learn. The reliability of these libraries has been extensively verified.

In this research, we use the K-Means method to process shear velocity variation data. The K-Means method aims to divide a dataset into  $k$  disjoint clusters by minimizing the inertia, which is defined as follows:

$$\sum_{i=1}^k \sum_{x_j \in M} (\|x_j - y_i\|^2) \quad \text{Equation 2.2}$$

where  $\|x_j - y_i\|$  is the distance between any data point in cluster  $M$  and the cluster center of cluster  $M$ .  $y_i$  is the arithmetic mean of all data points in cluster  $M$ .

In other words, according to the coherence of the data points within each cluster, the dataset is divided into separate clusters. By analyzing these clusters and associated parameters (e.g., cluster centers and cluster percentages used in this research), patterns in the dataset can be revealed. Compared to conventional methods, such as grouping a dataset

by its average value, the K-Means clustering method is different in terms of the statistical principle. In this study, it means that percentages of velocity clusters, as well as derived heterogeneity percentage profiles, are independent of the absolute values of shear velocity variations.

Specifically, the KMeans module from the scikit-learn package is applied in this research. Shear velocity variation data is grouped into two separate clusters, with clustering results consisting of clusters (a high velocity cluster and a low velocity cluster) and cluster centers. Clusters are used to calculate cluster percentages and construct global cluster maps. We can use global cluster maps to verify the accuracy of clusters. Cluster centers are used to generate cluster center charts. We can use cluster center charts to check the adequacy of extracting seismic data up to degree 60. Because of the correlation between clusters and cluster centers, we can also use cluster center charts to verify the consistency of clusters over depth and degree ranges.

#### 2.2.4 Heterogeneity percentage profiles

Before generating the heterogeneity percentage profile for a seismic model, the percentages of one cluster (the high velocity cluster or the low velocity cluster) at all depths must be calculated. The percentage of cluster  $M$  in the shear velocity variation dataset  $N$  is defined as:

$$a = m/n \quad \text{Equation 2.3}$$

where  $m$  and  $n$  are the numbers of data points in cluster  $M$  and shear velocity variation dataset  $N$ , respectively.

In this research, we select the high velocity cluster to compute cluster percentages. Cluster percentages for a seismic model are combined along depth to produce the model's heterogeneity percentage profile. We use heterogeneity percentage profiles at degree 60 to infer global mantle discontinuities. For each seismic model, by comparing its heterogeneity percentage profiles at degree 60 and a low degree, we can verify the model's stability at degree 60.

The K-Means method groups data based on coherence. It means that all heterogeneity percentage profiles generated in this research are independent of reference models and data types. In other words, for each seismic model, when we change its shear velocity data type or reference model, the model's heterogeneity percentage profile remains unchanged. Therefore, for all three seismic models, we can compare their heterogeneity percentage profiles directly.

### 2.3 Mantle convection modeling

Global seismic discontinuities in the mantle suggest dramatic heterogeneity changes at corresponding depths. There are possible viscosity jumps resulting from these changes. Viscosity jumps in the mantle control the movements of subduction slabs and mantle plumes. In this research, after identifying global mantle discontinuities, we investigate the possible viscosity jumps linked to discontinuities of interest.

#### 2.3.1 Governing equations

The numerical simulation of mantle convection has been extensively utilized to constrain the mantle's viscosity structure. In this study, we adopt the HC code based on (Hager & O'Connell, 1981) to explore the mantle's viscosity variations along depth. The



core function of the HC code is to solve the following three sets of governing equations for mantle flow:

$$\nabla \cdot v = 0 \quad \text{Equation 2.4}$$

$$\tau = -pI + 2\eta\varepsilon \quad \text{Equation 2.5}$$

$$0 = \nabla \cdot \tau + f \quad \text{Equation 2.6}$$

where  $v$  is the velocity,  $\tau$  is the stress tensor,  $p$  is the pressure,  $I$  is the identity matrix,  $\eta$  is the viscosity,  $\varepsilon$  is the strain rate tensor, and  $f$  is the body force.

### 2.3.2 Tomography and the mantle's density structure

When tomography is employed in numerical simulation, lateral viscosity variations have little effect on the predicted geoid (Ghosh, Becker, & Zhong, 2010). In other words, it is appropriate to invert the mantle's radial viscosity structure with the geoid by using tomography. In addition, the geoid is sensitive to viscosity in terms of relative changes (Hager & Richards, 1989). Mantle convection modeling with the geoid calculated from tomography is ideal for investigating viscosity jumps related to global mantle discontinuities.

In this study, the density structure of the mantle required by the HC code is derived from Model S362WMANI+M. Specifically, shear velocity variation data are transformed into density variation data. A constant scaling factor ( $d \ln \rho / d \ln V_s$ ) of 0.2 is used for the transformation.

### 2.3.3 The mantle's layer model and reference geoid

For mantle convection modeling, we are particularly interested in the possible viscosity jump in the middle mantle transition zone (MMTZ). With a layer model of the mantle, we can alter viscosity ratios between layers and then explore their influence on the global geoid. The mantle's layer model for this study is similar to the preferred model in (Liu & Zhong, 2016). It consists of five layers that represent major phase changes in minerals and stratifications of seismic velocity. We set viscosity ratios between layers 10 to 30 times and tested three combinations of viscosity ratios as listed in Table 2.1. In this research, the global geoid based on Model EGM2008 (Pavlis, Holmes, Kenyon, & Factor, 2012) is used as the reference geoid for comparison.

Table 2.1 Combinations of viscosity ratios for the mantle's layer model.

<b>Layer</b>	<b>Depth range (km)</b>	<b>Case 1</b>	<b>Case 2</b>	<b>Case 2</b>
1	0 - 100	10	10	10
2	100 - 660	1	1	1
3	660 - 1000	10	30	10
4	1000 - 1500	30	30	30
5	1500 - 2900	10	30	30

## CHAPTER 3. RESULTS

### 3.1 Seismic data and clustering results

In this research, we extract shear velocity variation data for all three seismic models (Models S362WMANI+M, SEMUCB-WM1, and S40RTS) up to harmonic degree 60. For the depth range of extraction, it is between 50 and 2850 km, with a 10 km interval. In addition, spectrum amplitude data up to degree 60 is extracted for each model. Seismic data (i.e., shear velocity variation data and spectrum amplitude data) are both obtained with the tool SeisTomoPy.

For shear velocity variation data at extremely low harmonic degrees, the K-Means clustering algorithm cannot guarantee the production of correct clustering results. For all three seismic models, clustering results (i.e., clusters and cluster centers) over a degree range of 3 to 60 are obtained. Clusters consist of a high velocity cluster and a low velocity cluster. Clusters are distinguished by their cluster centers. In this research, for all seismic models, the high velocity cluster is chosen to calculate cluster percentages and produce heterogeneity percentage profiles.

In this research, global shear velocity variation maps are compared with global cluster maps to verify the accuracy of clusters (see Figures 3.4–3.6). Spectrum amplitude charts (Figures 3.1–3.3) and cluster center charts (Figures 3.7–3.9) are generated for evaluating the adequacy of extracting seismic data up to degree 60. Cluster center charts are also used to verify the consistency of clusters across the degree and depth ranges. For all these maps and charts, when we exclude cases at extremely low harmonic degrees, correlated conclusions are unaffected. Consequently, for seismic data and clustering results

of all three models, the depth range is set from 50 to 2850 km with a 10 km interval, and the degree range is set from 3 to 60.

### 3.2 Spectrum amplitude charts

For all three seismic models, their spectrum amplitude distributions are displayed in spectrum amplitude charts (Figures 3.1–3.3). For each model, once the spectrum amplitude stabilizes, indicating that the model has reached stable status, additional degrees do not affect its clustering results. For Model S362WMANI+M, as depicted in Figure 3.1, the spectrum amplitude stabilizes (damps towards 0) before degree 24, which is the upper limit of the model's spectral range. A similar occurrence happens to Model S40RTS with a spectral range up to degree 40, where its spectrum amplitude stabilizes before degree 40. This is demonstrated in Figure 3.2. As shown in Figure 3.3 for Model SEMUCB-WM1, whose spectral range is up to degree 96, its spectrum amplitude stabilizes before degree 60.

The main objective of this research is to identify global mantle discontinuities. All three seismic models become stable before degree 60. For K-Means clustering, components of degrees higher than 60 do not make any difference to the results. It is adequate to extract seismic data up to degree 60 for all three models.

### 3.3 Global cluster maps and global shear velocity variation maps

To evaluate the accuracy of clusters, global cluster maps and global shear velocity variation maps are generated for all three seismic models. For every model, by comparing its global cluster maps to related global shear velocity variation maps (see Figures 3.4–3.6), it is confirmed that at various depths and harmonic degrees, clusters (the high velocity

cluster and the low velocity cluster) accurately depict the distribution of shear velocity variations in the mantle.

In Figures 3.4–3.6, low harmonic degrees of 20, 35, and 40 are intentionally chosen for Models S362WMANI+M, S40RTS, and SEMUCB-WM1, respectively. The degree 60 is also picked for all three models. For each model, its heterogeneity percentage profiles at the chosen low degree and degree 60 are compared to verify the stability of the model at degree 60 (see Figures 3.13–3.15). Global mantle discontinuities are inferred from key cluster percentage shifts in heterogeneity percentage profiles at degree 60 (Figures 3.16–3.18). For all three models, the accuracy of clusters at degrees of interest is confirmed here.

### 3.4 Cluster center charts

Before calculating cluster percentages and constructing heterogeneity percentage profiles with the high velocity cluster, it is important to confirm that clusters are consistent over depth and degree ranges. Clusters are distinguished by their cluster centers. Therefore, the consistency of clusters can be verified with cluster center charts.

As shown in Figures 3.7–3.9, cluster center charts are created for all three seismic models. At every depth, there is no intersection or flip between two lines representing cluster centers. At every harmonic degree, there is no switching between cluster center pairs. Cluster centers are consistent across depth and degree ranges. Accordingly, the consistency of clusters is confirmed.

In Figures 3.7 and 3.8, lines representing cluster centers flatten off before degrees 24 and 40, the upper limits of spectral ranges for Models S362WMANI+M and S40RTS. As shown in Figure 3.9, for Model SEMUCB-WM1 with a spectral range up to degree 96, lines representing cluster centers flatten off before degree 60. All charts indicate that three

seismic models become stable before harmonic degree 60. Therefore, it is appropriate to extract seismic data only up to degree 60 in this research.

### 3.5 Heterogeneity percentage profiles

Cluster percentages are combined along depth to generate heterogeneity percentage profiles. Discontinuities are inferred from abrupt shifts in these profiles. In this research, our primary objective is to identify global discontinuities in the mantle. Global mantle discontinuities are inferred from key cluster percentage shifts. They indicate significant changes in the mantle's heterogeneity.

#### 3.5.1 Data types and reference models

For any seismic model, when changing its shear velocity data type or reference model, cluster centers change accordingly. But heterogeneity percentage profiles stay intact. Examples are shown in Figures 3.10 and 3.11. Unchanged heterogeneity percentage profiles reveal the statistical principle behind the K-Means clustering method: grouping data based on coherence, not absolute value.

SeisTomoPy only supports the extraction of shear velocity variation data relative to the default reference model. In order to generate Figures 3.10 and 3.11 for Models S362ANI+M and SEMUCB-WM1, we retrieve shear velocity data and shear velocity variation data relative to the default reference model from GitHub<sup>2</sup>. Similar to the production of Figure 1.1, the same algorithm for isotropic PREM is used to calculate shear velocities. It should be noted that Model S362ANI+M, the upper-mantle version of Model S362WMANI+M, is used to produce Figure 3.10.

---

<sup>2</sup><https://github.com/shuleyu/seismic-tomography-models>

### 3.5.2 Geophysical significance of abrupt cluster percentage shifts

Heterogeneity percentage profiles are independent of the reference model and data type. Therefore, they can be compared directly among different models. But it is meaningless to compare cluster percentages. As demonstrated in Figure 3.12, because different datasets and inversion methods are used to create three seismic models, global cluster maps for these models at chosen depths are dissimilar. Accordingly, the comparison of cluster percentages between models is pointless. However, in the heterogeneity percentage profile for each seismic model, noticeable alterations in cluster percentage indicate dramatic changes in the mantle's heterogeneity along depth (i.e., mantle discontinuities). Abrupt cluster percentage shifts have geophysical significance and can be compared among models.

In heterogeneity percentage profiles, abrupt cluster percentage shifts are displayed in two different ways: turn and gradient. In the first way, cluster percentage changes from increasing to decreasing, or vice versa. In the second way, when cluster percentage increases, it changes from increasing rapidly to slowly, or vice versa. Similarities exist when the cluster percentage decreases.

### 3.5.3 Global mantle discontinuities inferred from key cluster percentage shifts

In Figures 3.13–3.15, for each model, when comparing its heterogeneity percentage profiles at the chosen low degree and degree 60, the similarity between profiles indicates that the model has been stable before either the upper limit of its spectra range (degree 24 for Models S362WMANI+M and degree 40 for Model S40RTS) or degree 60 (Model SEMUCB-WM1). All seismic models extracted at degree 60 are stable. Therefore, discontinuities inferred from heterogeneity percentage profiles at harmonic degree 60 are



reliable. Because of the intrinsic differences between three seismic models, the abrupt cluster percentage shifts shown in the heterogeneity percentage profile for one model may not be noticeable in the profiles for other models. Even when an abrupt shift is recognized clearly in all three profiles, it may be displayed differently.

We aim to identify global discontinuities in the mantle. To avoid bias from a specific seismic model, key cluster percentage shifts are used to infer global mantle discontinuities. A key cluster percentage shift is an abrupt shift that is noticeable in all three heterogeneity percentage profiles at harmonic degree 60. Global mantle discontinuities at depths of 400 km, 650 km, 1050 km, 1500 km, and 2700 km are deduced from heterogeneity percentage profiles. It should be noted that all global mantle discontinuities can still be recognized clearly after reducing the depth resolution of profiles by increasing the interval from 10 km to 50 km (see Figures 3.16–3.18).

In the heterogeneity percentage profile for Model S362WMANI+M (Figure 3.16), at around 400 km, the cluster percentage stops decreasing. At around 650 km, the cluster percentage decreases sharply and then starts to increase. At around 1050 km, the cluster percentage starts to increase rapidly. At around 1500 km, the cluster percentage stops decreasing. At around 2700 km, the cluster percentage changes from increasing to decreasing.

In the heterogeneity percentage profile for Model S40RTS (Figure 3.17), at around 400 km, the cluster percentage changes from decreasing rapidly to slowly. At around 650 km, the cluster percentage changes from decreasing to increasing. At around 1050 km, the cluster percentage stops decreasing. At around 1500 km, the cluster percentage starts to increase. At around 2700 km, the cluster percentage stops decreasing.

In the heterogeneity percentage profile for Model SEMUCB-WM1 (Figure 3.18), at around 400 km, the cluster percentage stops decreasing. At around 650 km, 1050 km, and 1500 km, the cluster percentage changes from decreasing to increasing. At around 2700 km, the cluster percentage changes from increasing to decreasing.

#### 3.5.4 Other discontinuities in the mantle

Except for the above global mantle discontinuities, there are other mantle discontinuities indicated by cluster percentage shifts. A typical example is the shift at around 900 km. As shown in Figures 3.13–3.15, this shift is detectable in all three heterogeneity percentage profiles. However, in the profiles for Models S362WMANI+M and S40RTS (Figures 3.13 and 3.14), it is not as sharp as key cluster percentage shifts. Therefore, the inferred 900 km discontinuity is not a global discontinuity.

In heterogeneity percentage profiles for Models S362WMANI+M and SEMUCB-WM1 (Figures 3.13 and 3.15), we can observe an abrupt shift in the depth range of the lower mantle. The cluster percentage changes markedly between 2200 km and 2600 km in the heterogeneity percentage profile of Model S40RTS (Figure 3.14). This indicates a global discontinuity in the lower mantle. However, we are unable to determine the exact depth of this discontinuity at this time.

#### 3.6 Modeled geoid maps

We conducted mantle convection modeling with three different viscosity ratio combinations. Correlations between the modeled geoid and the global geoid are listed in Table 3.1. As shown in Figures 3.19–3.21, modeled geoid maps are also created to compare with the global geoid map.

Table 3.1 Correlation results for modeling with different viscosity ratio combinations.

<b>Layer</b>	<b>Depth range (km)</b>	<b>Case 1</b>	<b>Case 2</b>	<b>Case 2</b>
1	0 - 100	10	10	10
2	100 - 660	1	1	1
3	660 - 1000	10	30	10
4	1000 - 1500	30	30	30
5	1500 - 2900	10	30	30
<b>Correlation</b>		0.44	0.69	0.74

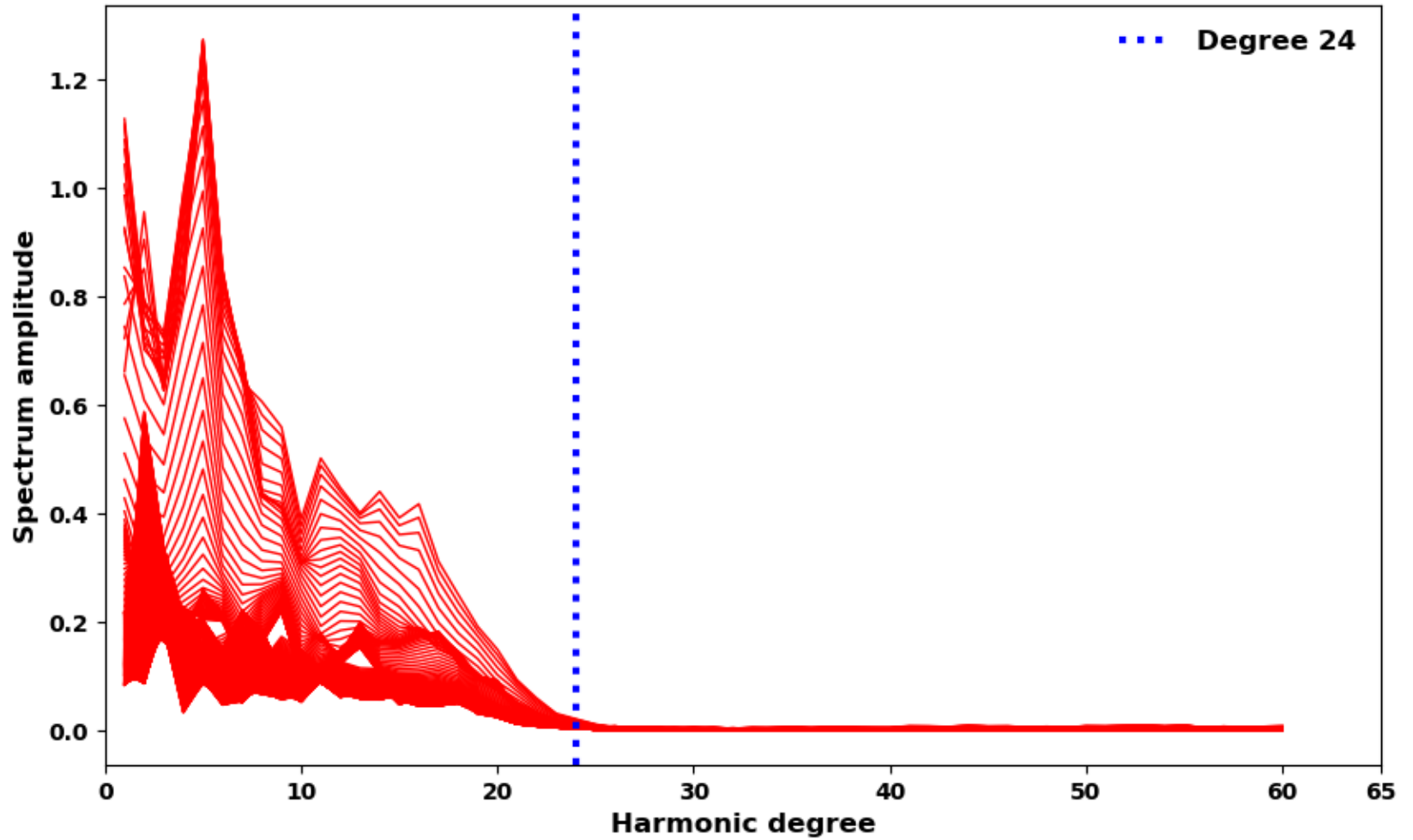


Figure 3.1 Spectrum amplitude chart for Model S362WMANI+M. Lines represent spectrum amplitude distributions at various depths. The spectral range of Model S362WMANI+M is up to degree 24.

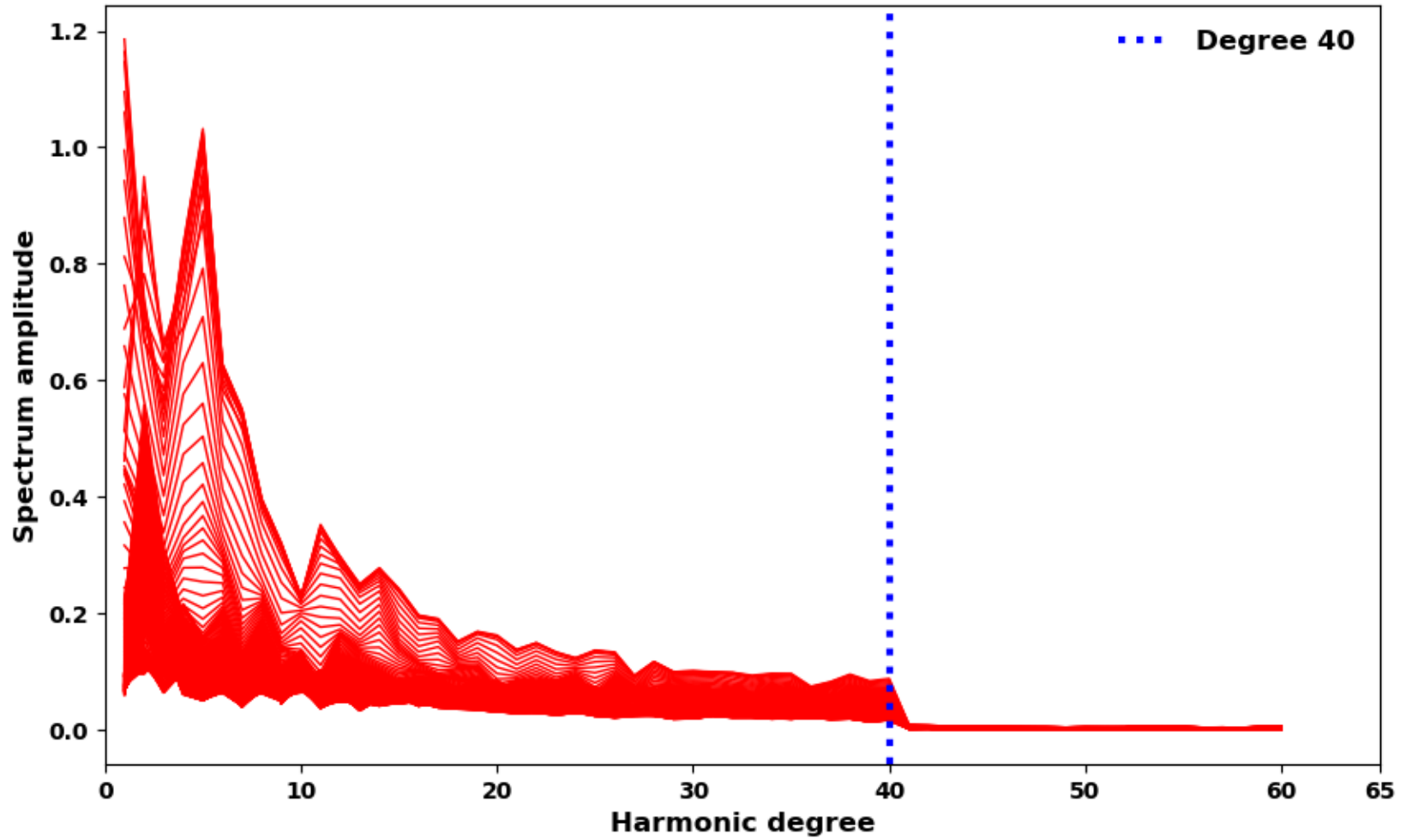


Figure 3.2 Spectrum amplitude chart for Model S40RTS. Lines represent spectrum amplitude distributions at various depths. The spectral range of Model S40RTS is up to degree 40.

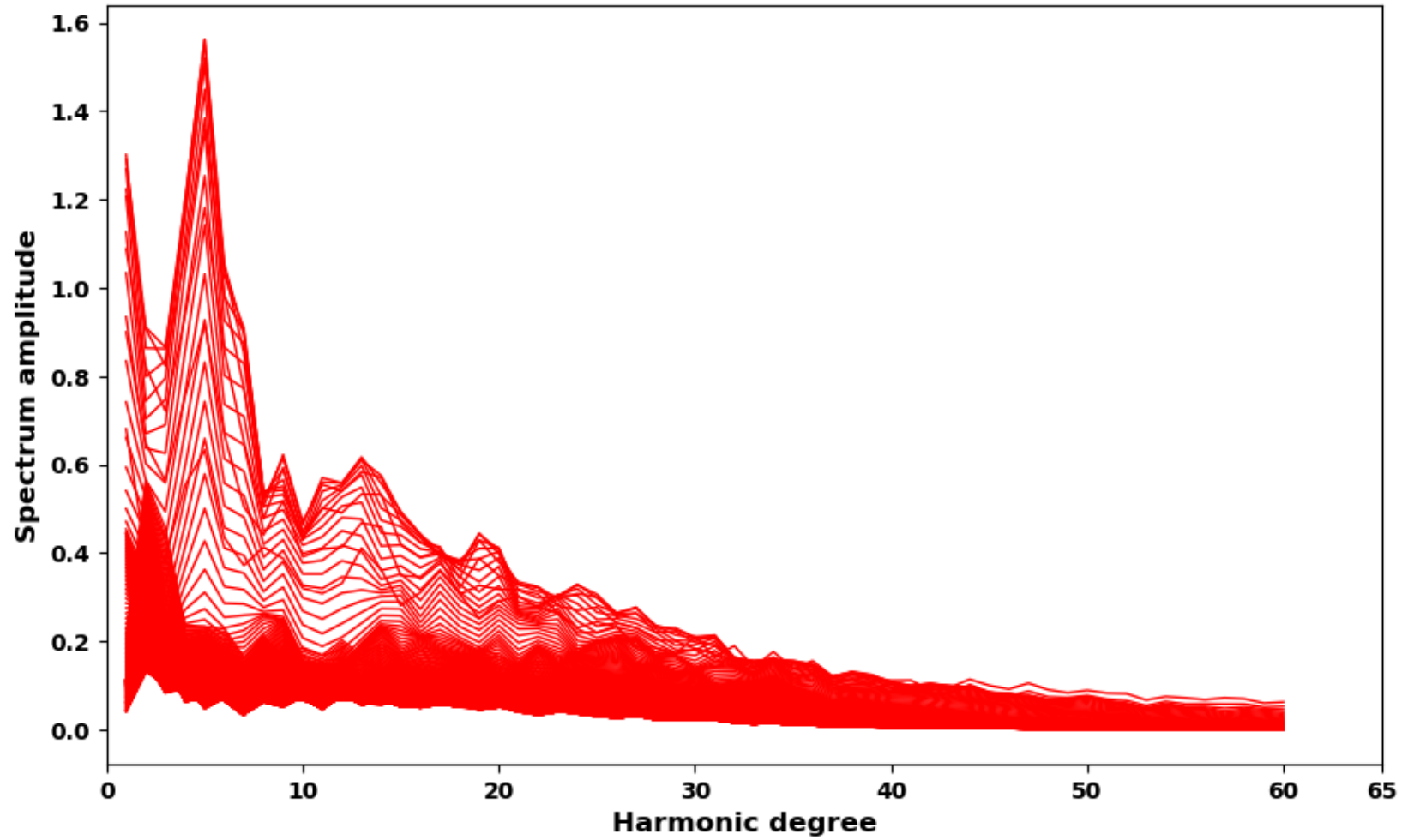


Figure 3.3 Spectrum amplitude chart for Model SEMUCB-WM1. Lines represent spectrum amplitude distributions at various depths. The spectral range of Model SEMUCB-WM1 is up to degree 96.

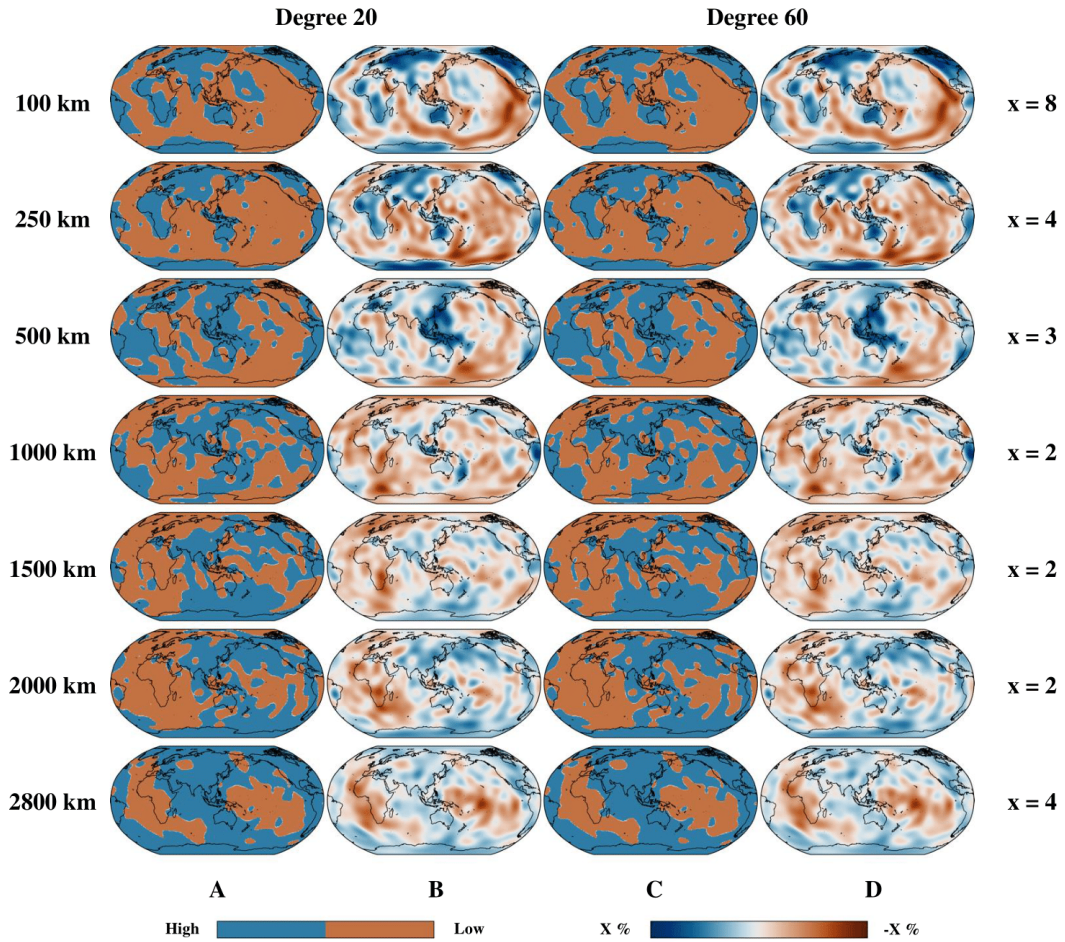


Figure 3.4 Global cluster maps and global shear velocity variation maps for Model S362WMANI+M. Global cluster maps are in Columns A and C. Global shear velocity variation maps are in Columns B and D. Maps at degree 20 are in Columns A and B. Maps at degree 60 are in Columns C and D. Clusters accurately reflect the geospatial distribution of shear velocity variations.



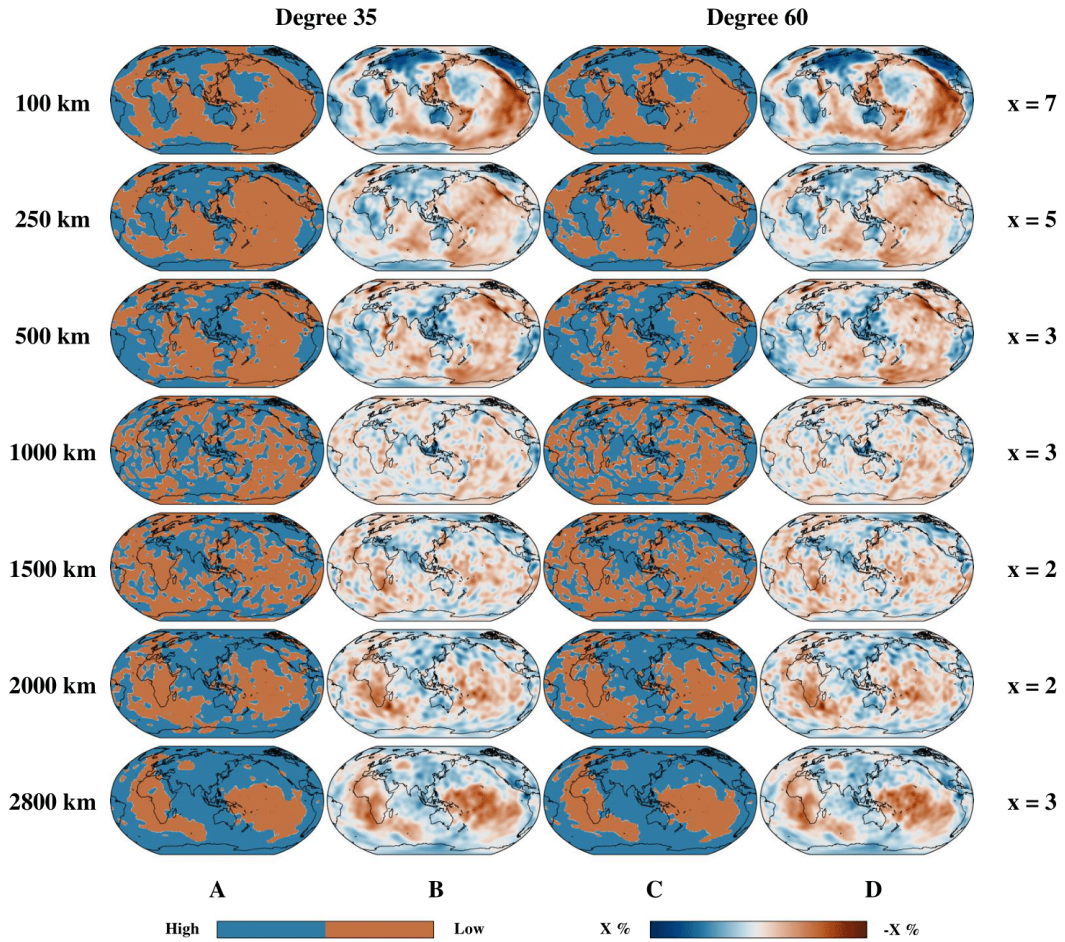


Figure 3.5 Global cluster maps and global shear velocity variation maps for Model S40RTS. Global cluster maps are in Columns A and C. Global shear velocity variation maps are in Columns B and D. Maps at degree 35 are in Columns A and B. Maps at degree 60 are in Columns C and D. Clusters accurately reflect the geospatial distribution of shear velocity variations.



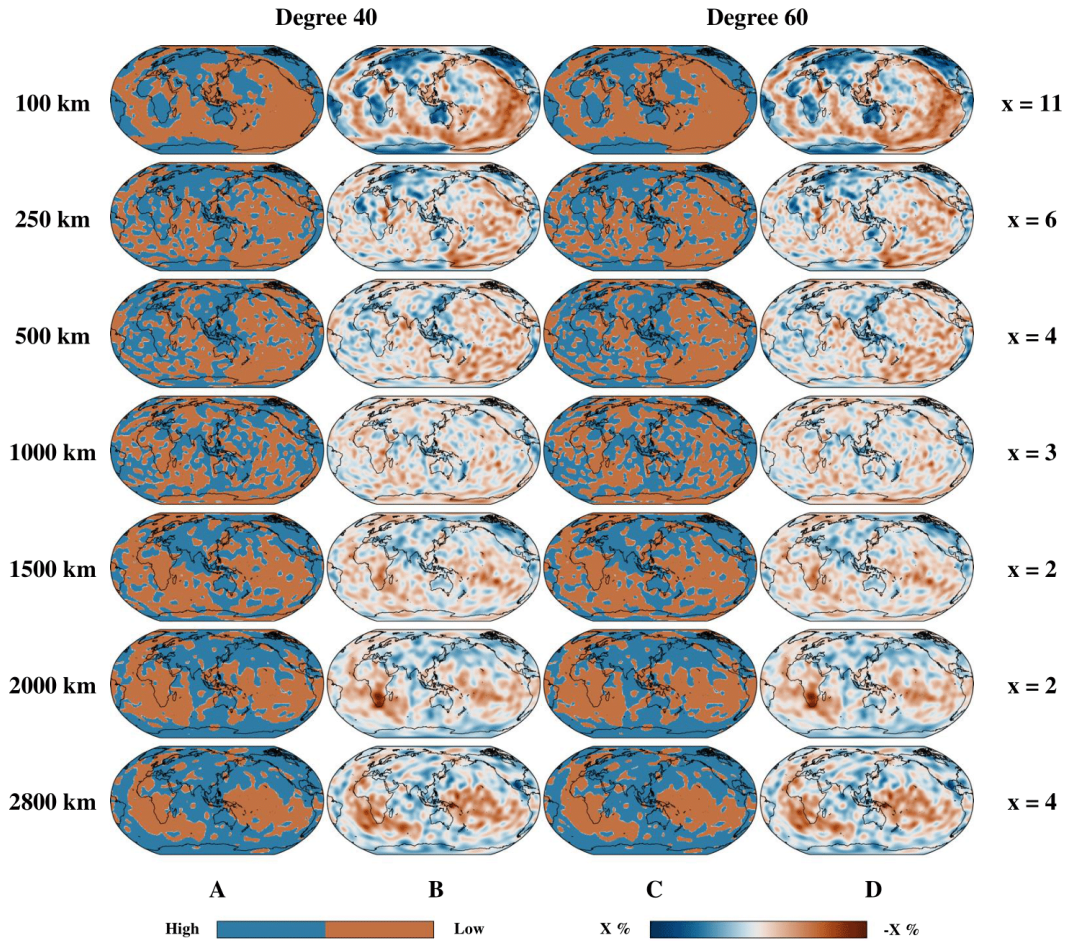


Figure 3.6 Global cluster maps and global shear velocity variation maps for Model SEMUCB-WM1. Global cluster maps are in Columns A and C. Global shear velocity variation maps are in Columns B and D. Maps at degree 40 are in Columns A and B. Maps at degree 60 are in Columns C and D. Clusters accurately reflect the geospatial distribution of shear velocity variations.

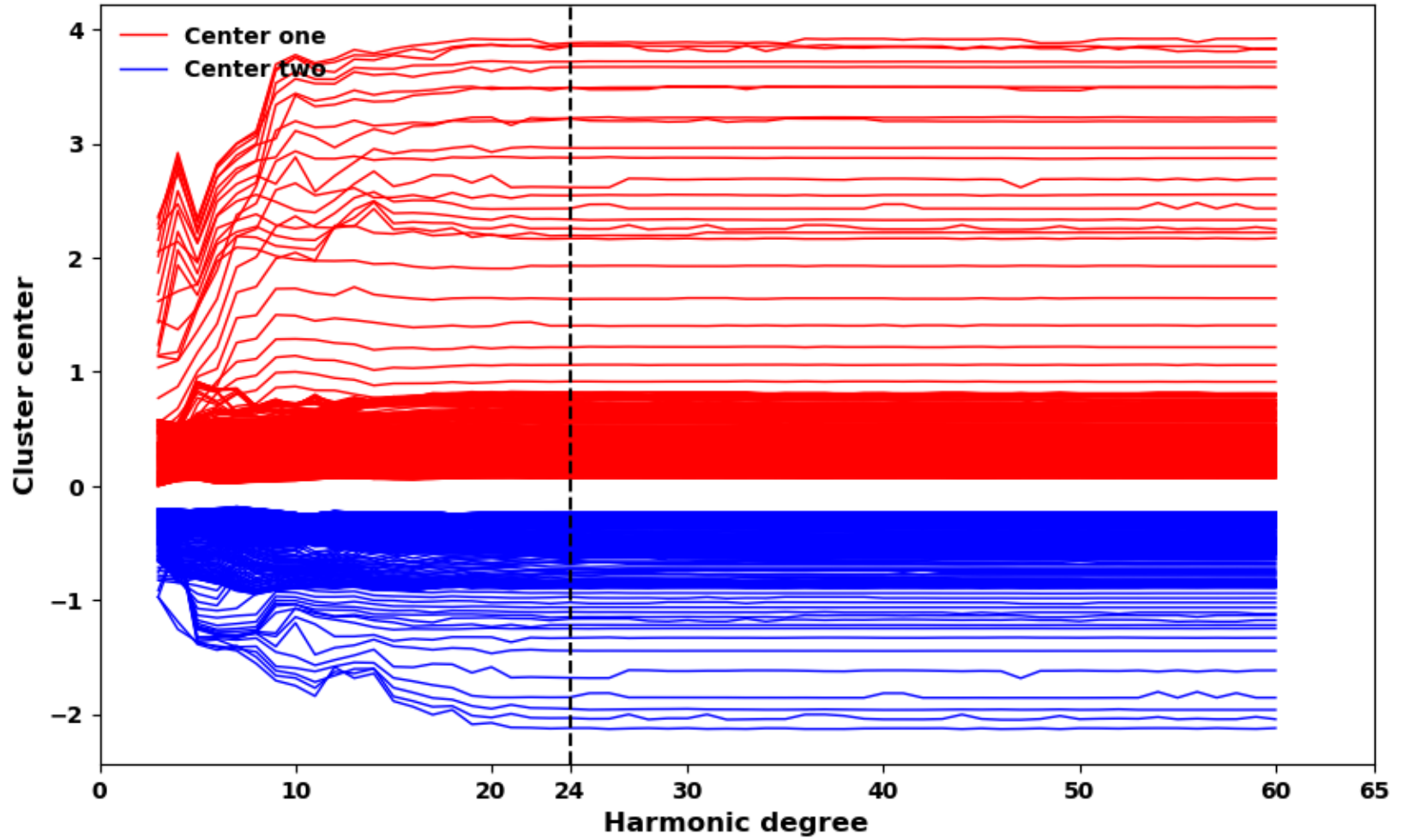


Figure 3.7 Cluster center chart for Model S362WMANI+M. Lines represent two cluster centers at various depths.

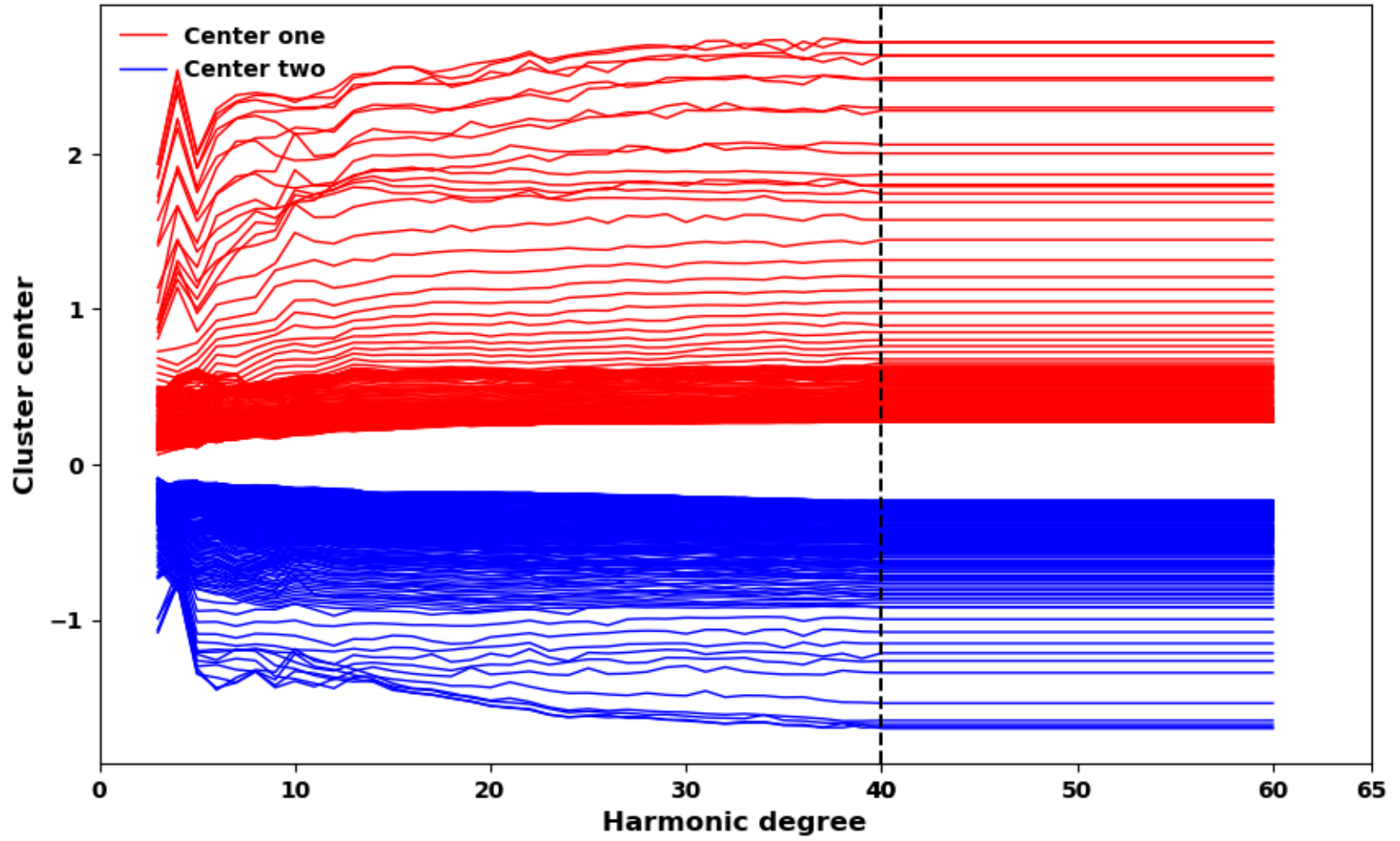


Figure 3.8 Cluster center chart for Model S40RTS. Lines represent two cluster centers at various depths.

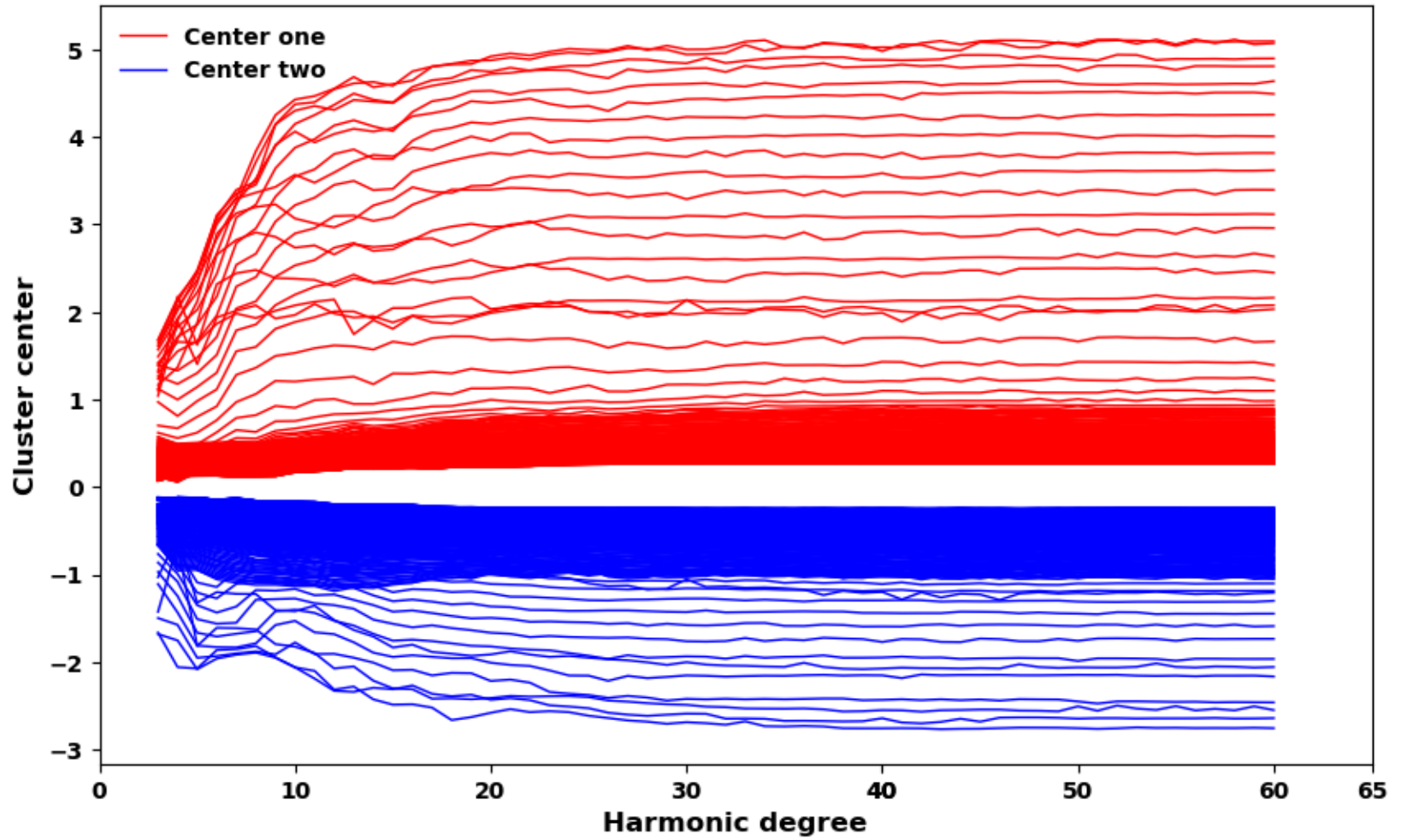


Figure 3.9 Cluster center chart for Model SEMUCB-WM1. Lines represent two cluster centers at various depths.

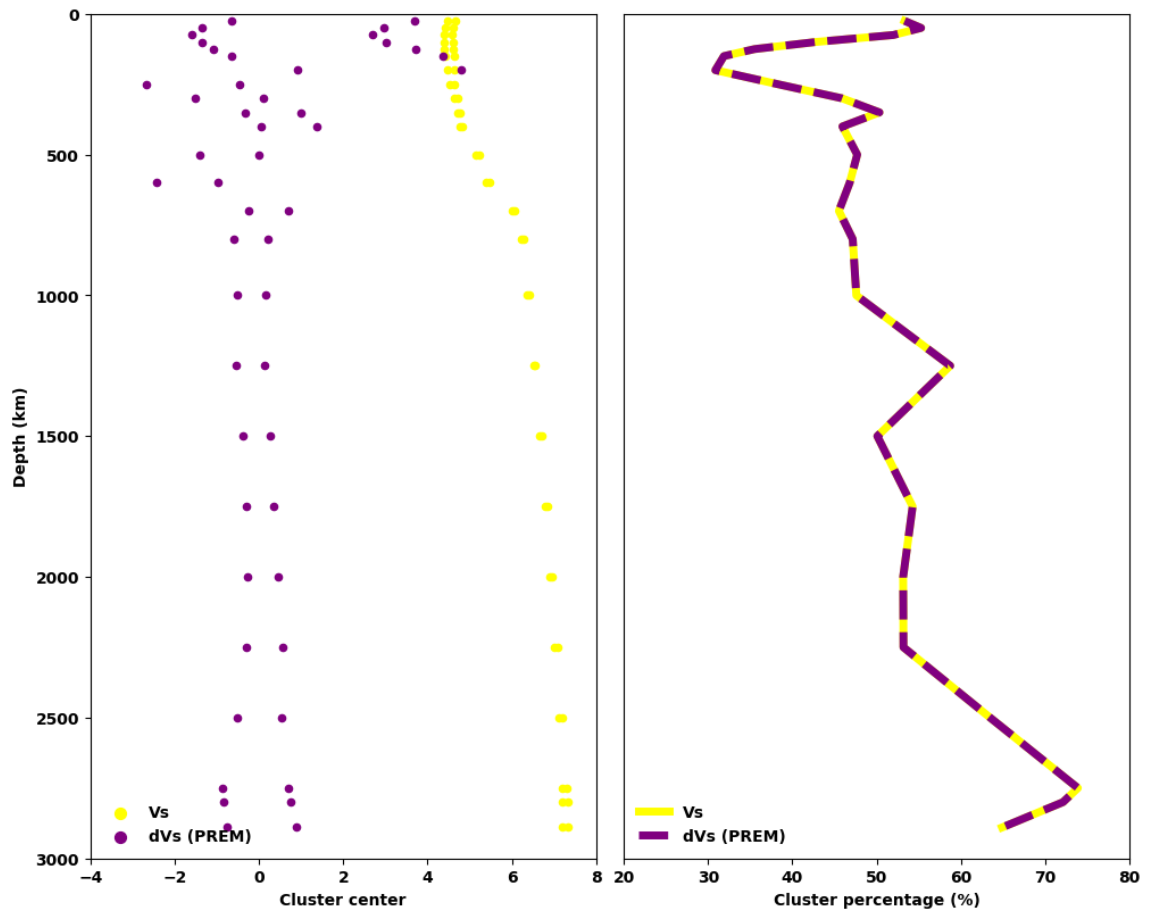


Figure 3.10 Cluster center profiles and heterogeneity percentage profiles for Model S362ANI+M.  $V_s$ ,  $dV_s$  (PREM) represent shear velocity and shear velocity variation relative to PREM, respectively. Heterogeneity percentage profiles do not depend on the data type or reference model.

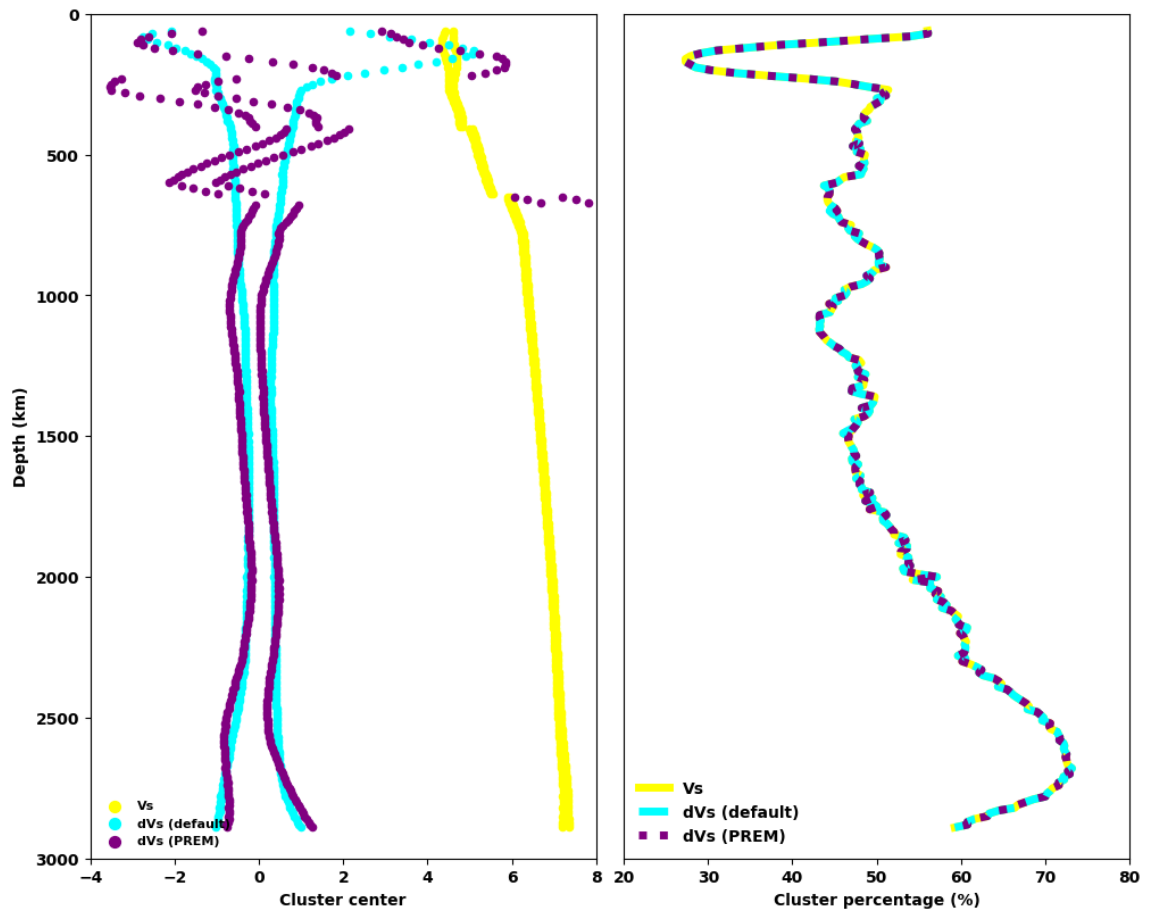


Figure 3.11 Cluster center profiles and heterogeneity percentage profiles for Model SEMUCB-WM1.  $V_s$ ,  $dV_s$  (default), and  $dV_s$  (PREM) represent shear velocity, shear velocity variation relative to the default reference model, and shear velocity variation relative to PREM, respectively. Heterogeneity percentage profiles do not depend on the data type or reference model.



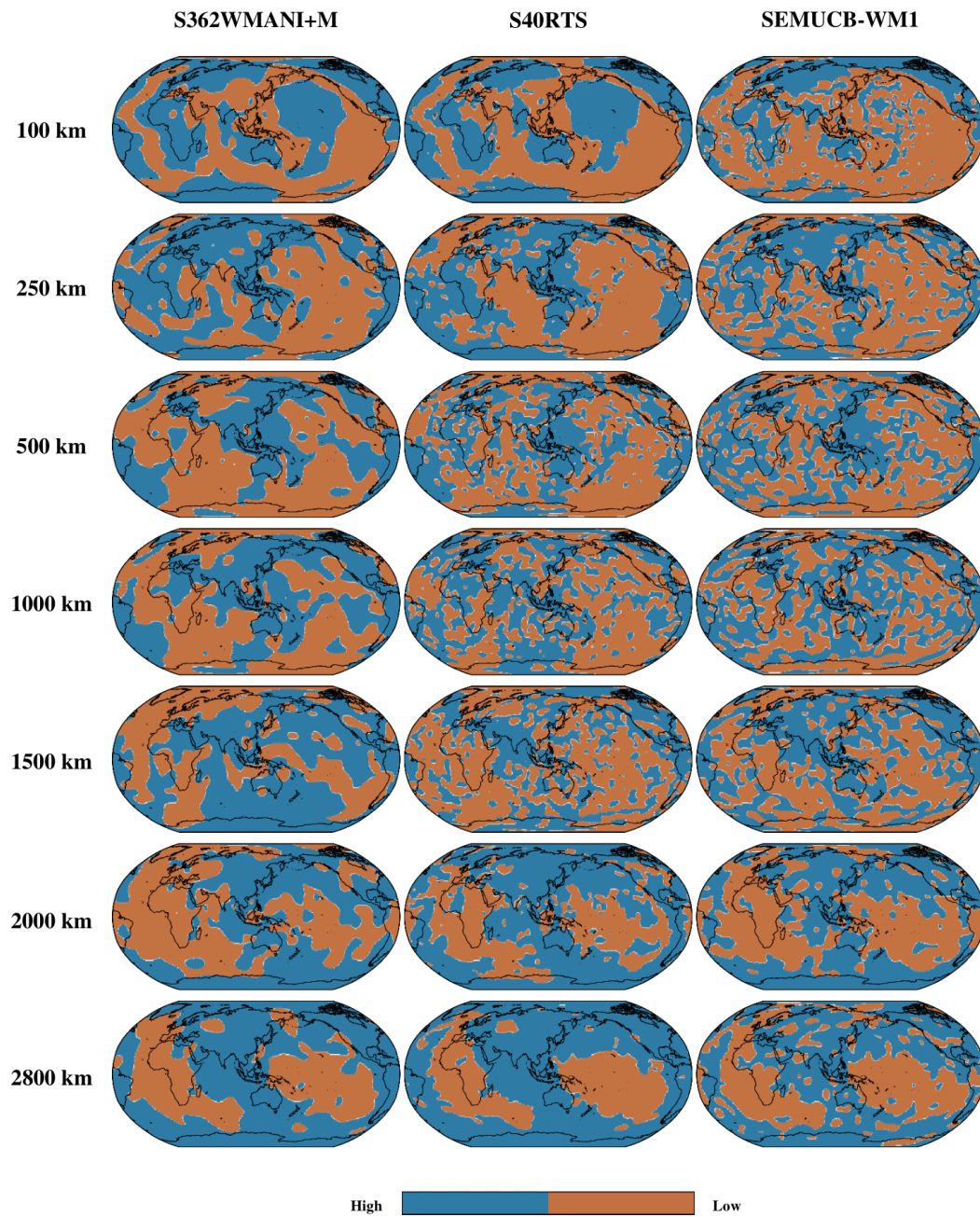


Figure 3.12 Global cluster maps at degree 60 for all three seismic models. Maps are dissimilar among models at the same depths.

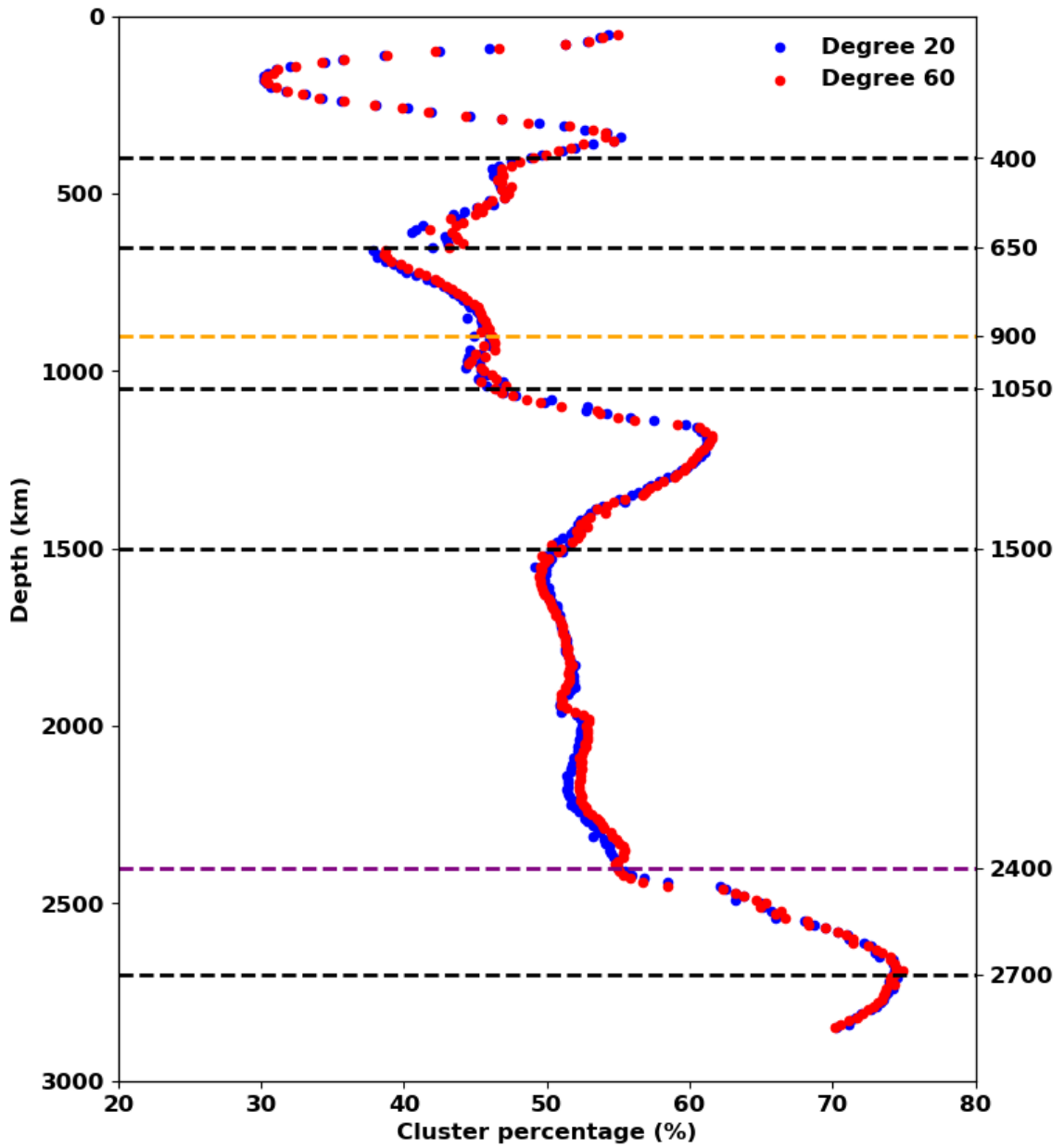


Figure 3.13 Heterogeneity percentage profiles at degrees 20 and 60 for Model S362WMANI+M. Global mantle discontinuities are denoted by black dashed lines. The abrupt cluster percentage shift at around 2400 km indicates a discontinuity in the lower mantle.



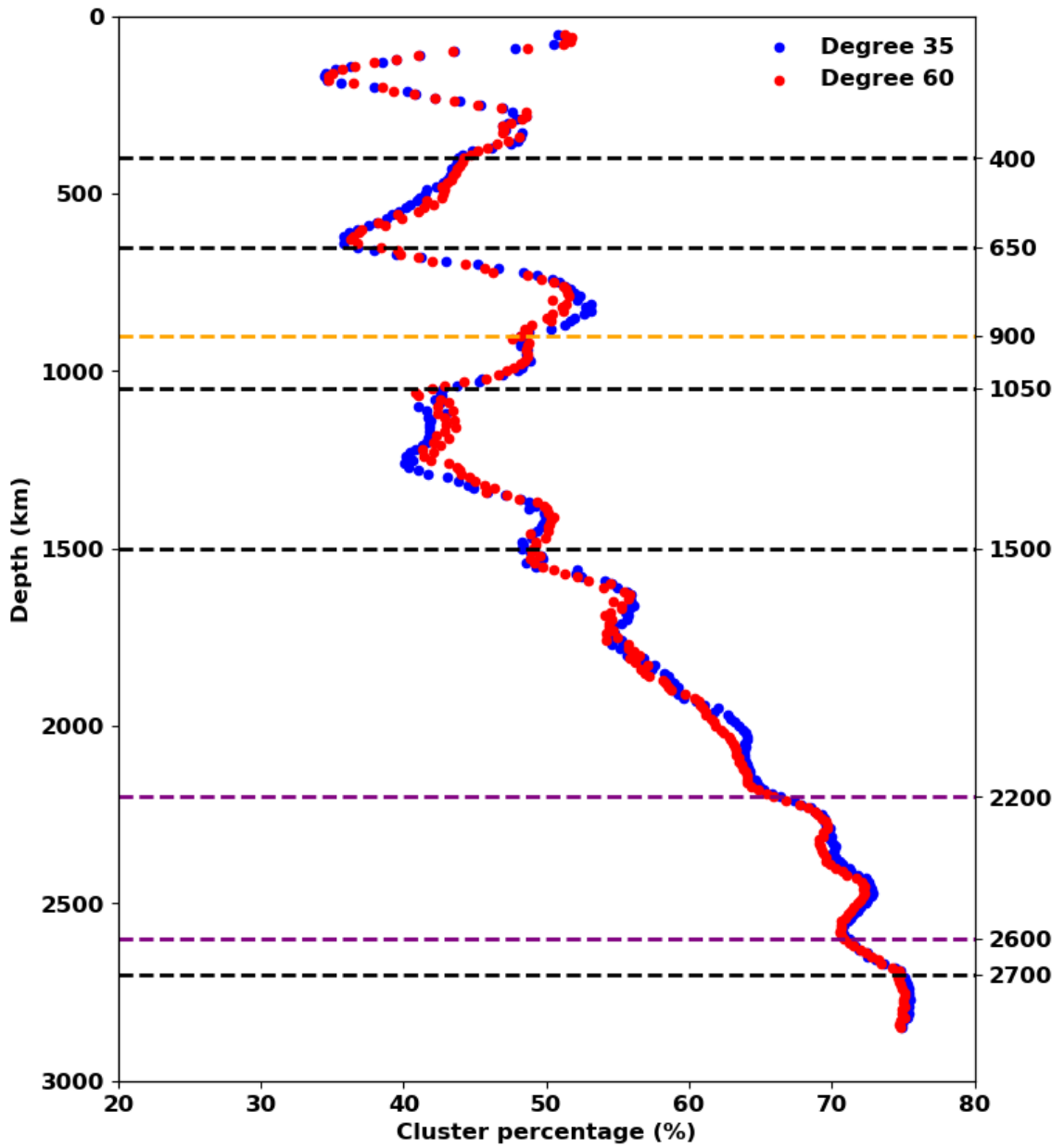


Figure 3.14 Heterogeneity percentage profiles at degrees 35 and 60 for Model S40RTS. Global mantle discontinuities are denoted by black dashed lines. The cluster percentage changes markedly between 2200 km and 2600 km.

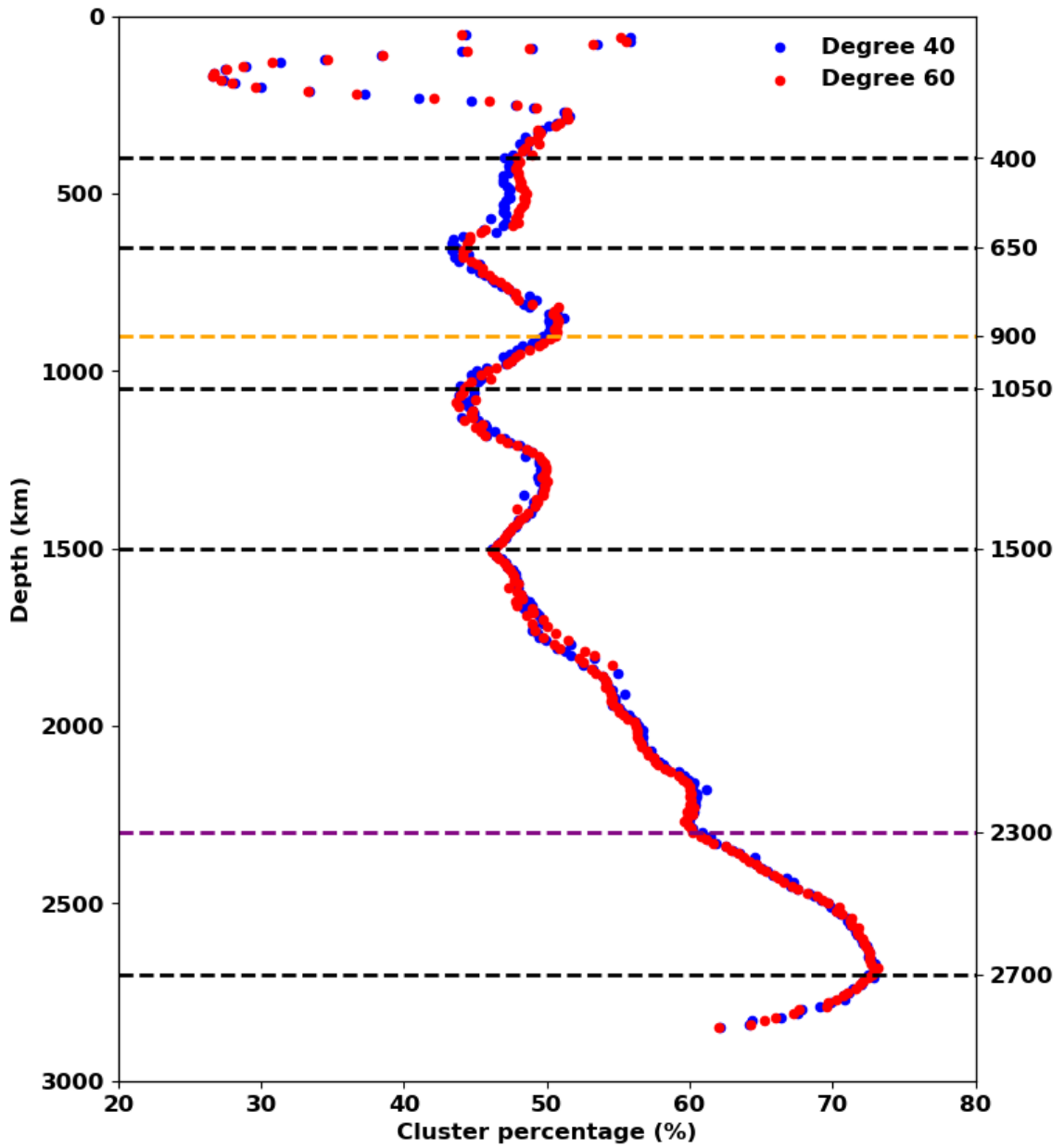


Figure 3.15 Heterogeneity percentage profiles at degrees 40 and 60 for Model SEMUCB-WM1. Global mantle discontinuities are denoted by black dashed lines. The abrupt cluster percentage shift at around 2300 km indicates a discontinuity in the lower mantle.

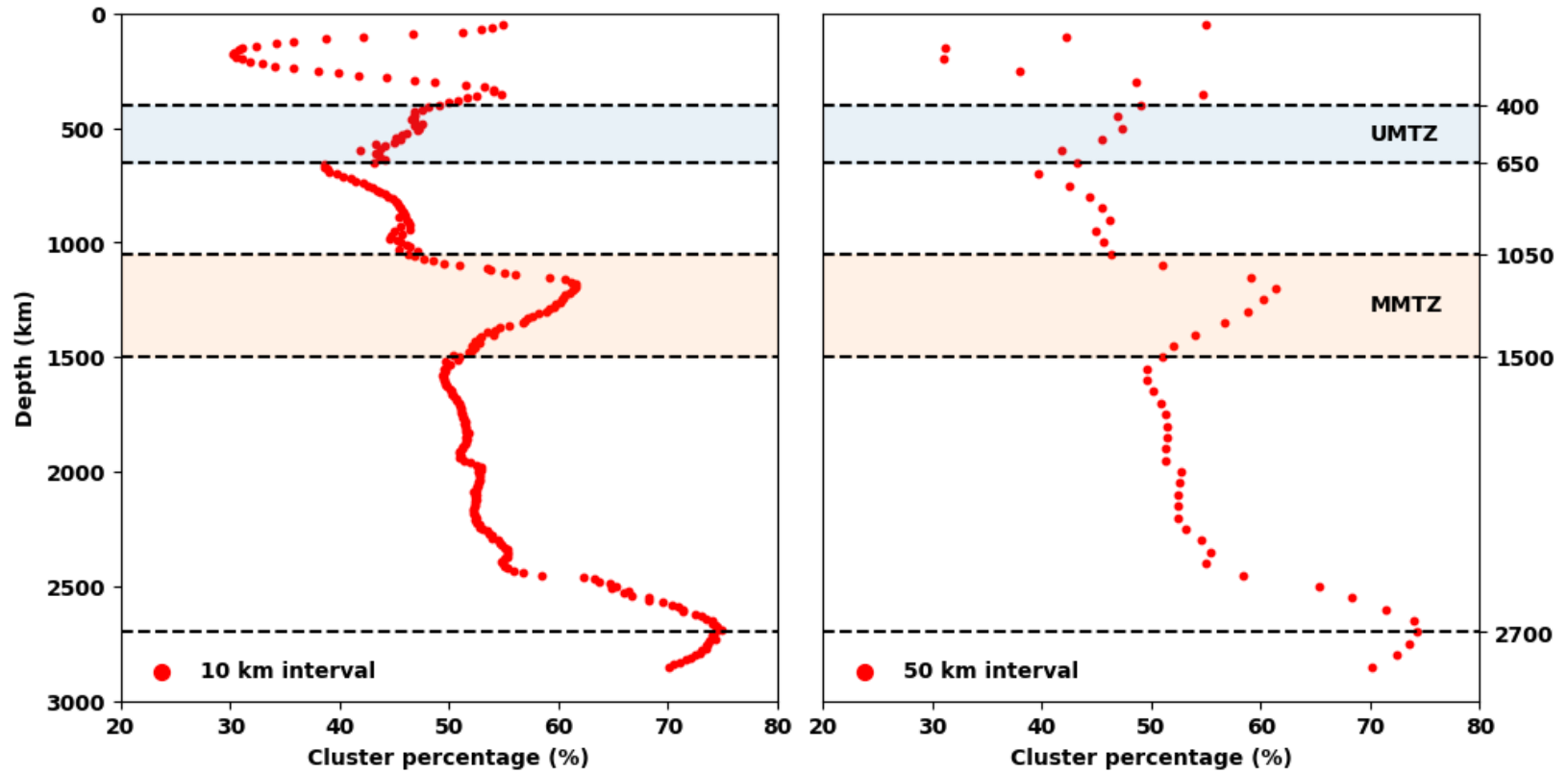


Figure 3.16 Heterogeneity percentage profiles at degree 60 for Model S362WMANI+M. Global mantle discontinuities are denoted by black dashed lines. The upper mantle transition zone (UMTZ) and middle mantle transition zone (MMTZ) are denoted by different colors.

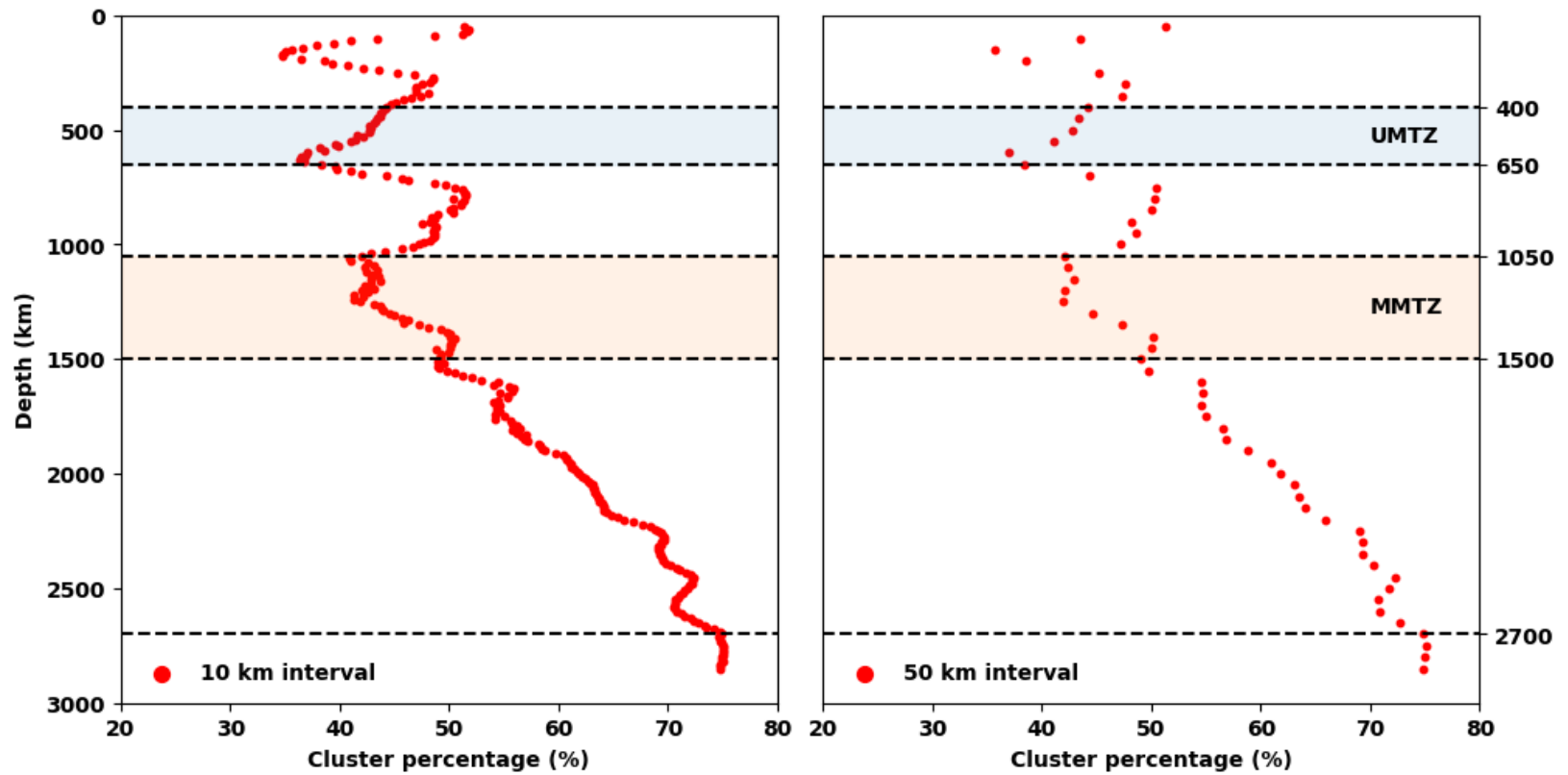


Figure 3.17 Heterogeneity percentage profiles at degree 60 for Model S40RTS. Global mantle discontinuities are denoted by black dashed lines. The upper mantle transition zone (UMTZ) and middle mantle transition zone (MMTZ) are denoted by different colors.

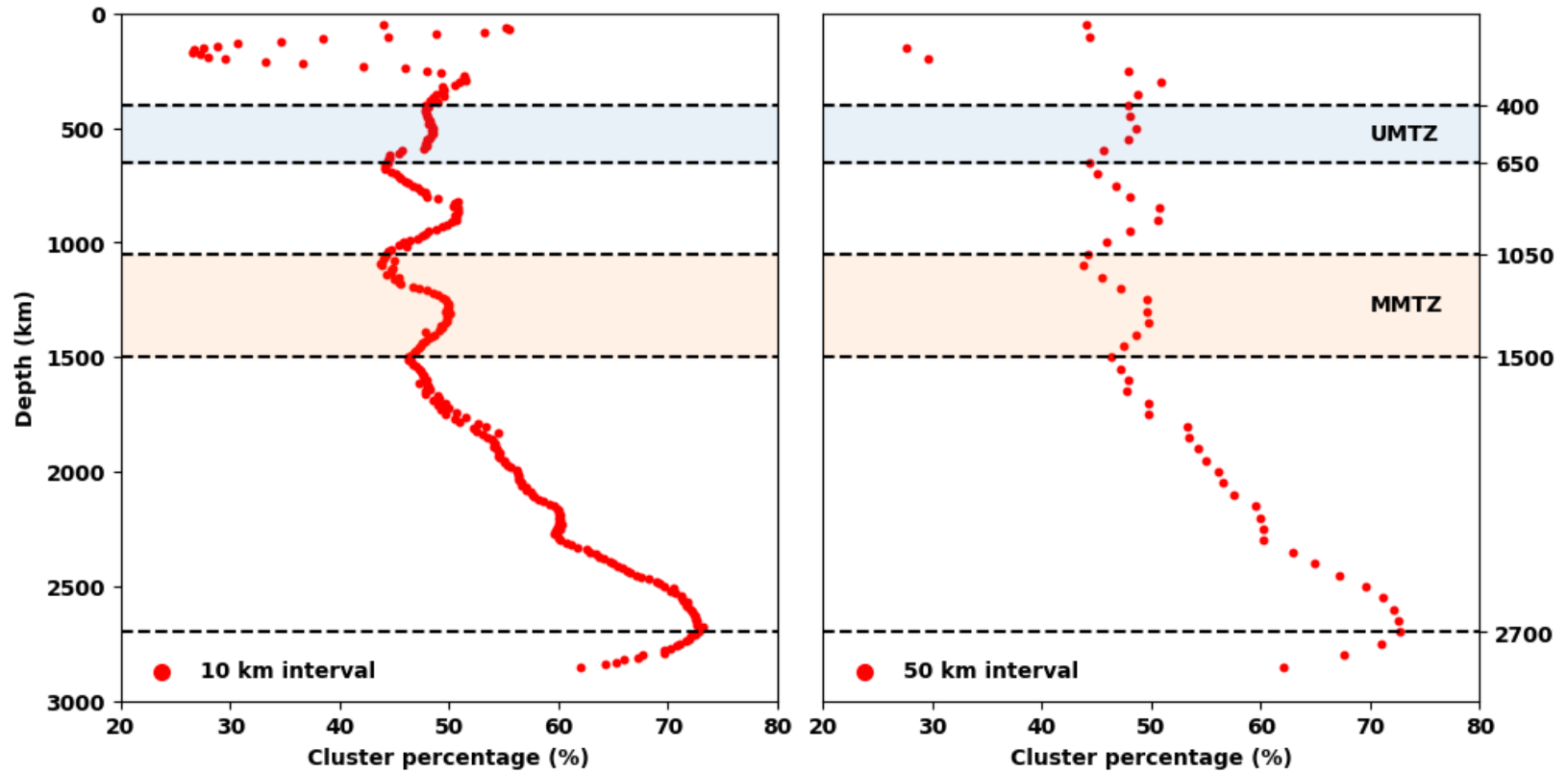
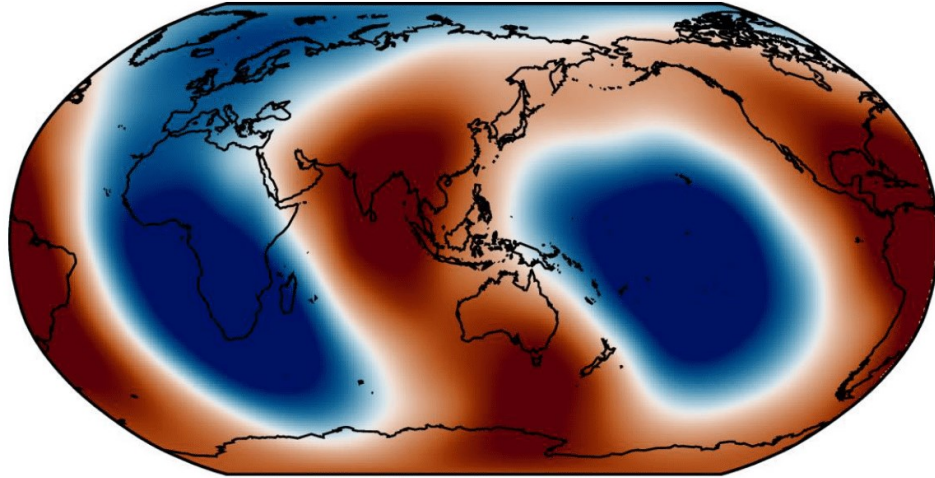
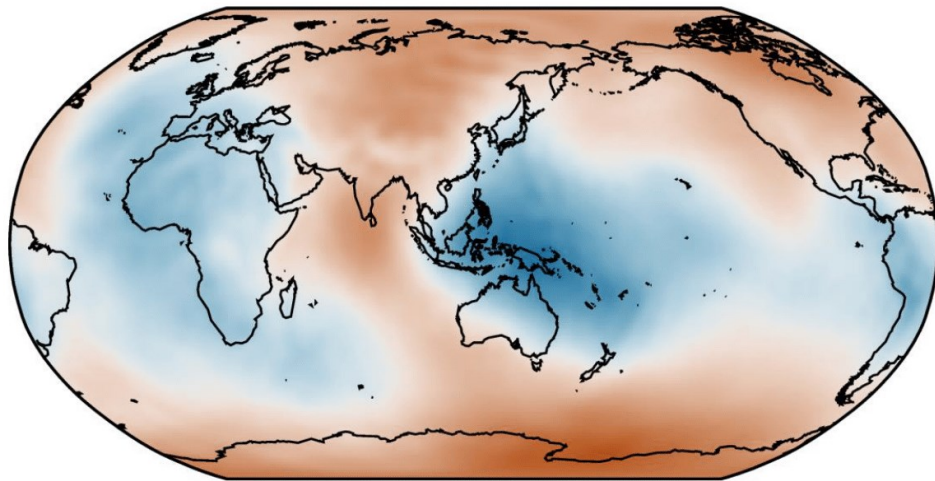


Figure 3.18 Heterogeneity percentage profiles at degree 60 for Model SEMUCB-WM1. Global mantle discontinuities are denoted by black dashed lines. The upper mantle transition zone (UMTZ) and middle mantle transition zone (MMTZ) are denoted by different colors.

**Modeled Geoid**



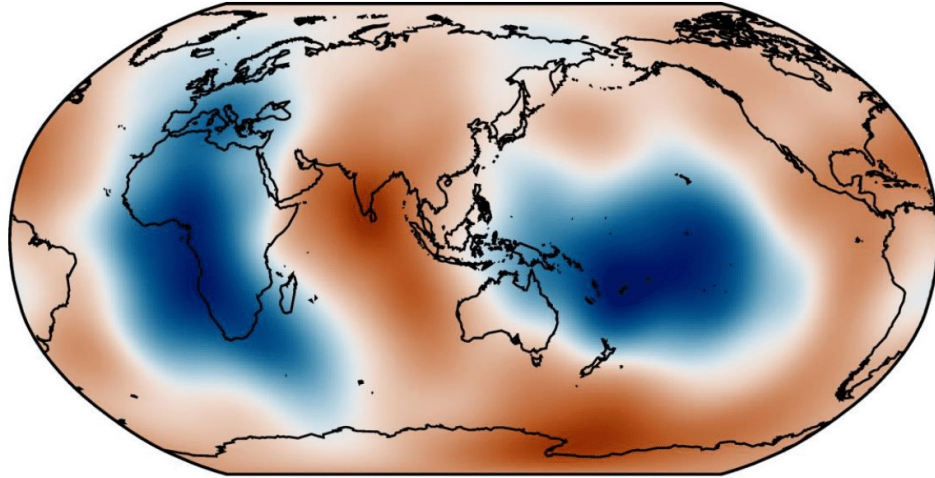
**Global Geoid**



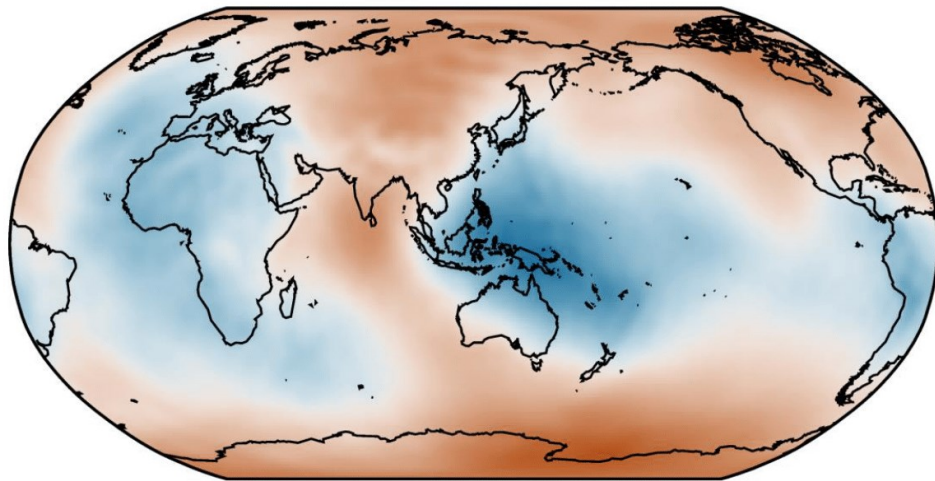
200 m  - 200 m

Figure 3.19 Modeled geoid map for Case 1. The correlation (fit) is 0.44.

**Modeled Geoid**



**Global Geoid**

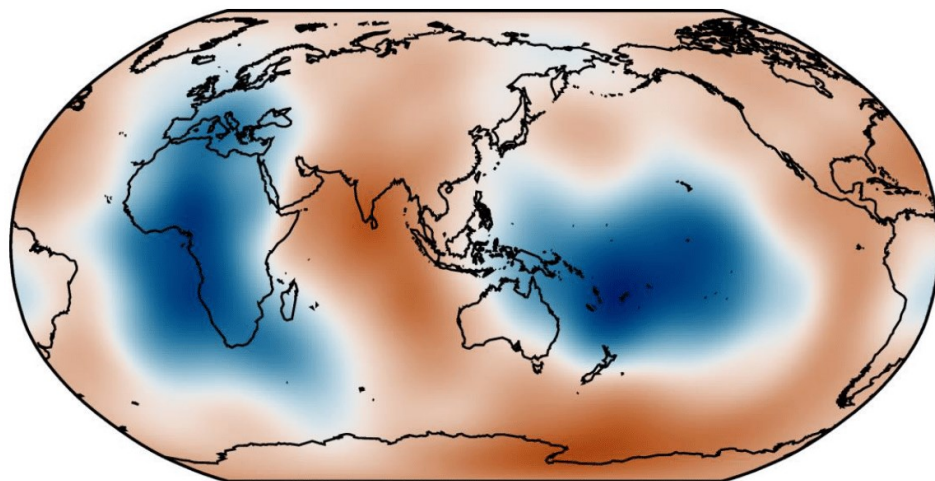


200 m  - 200 m

Figure 3.20 Modeled geoid map for Case 2. The correlation (fit) is 0.69.



**Modeled Geoid**



**Global Geoid**

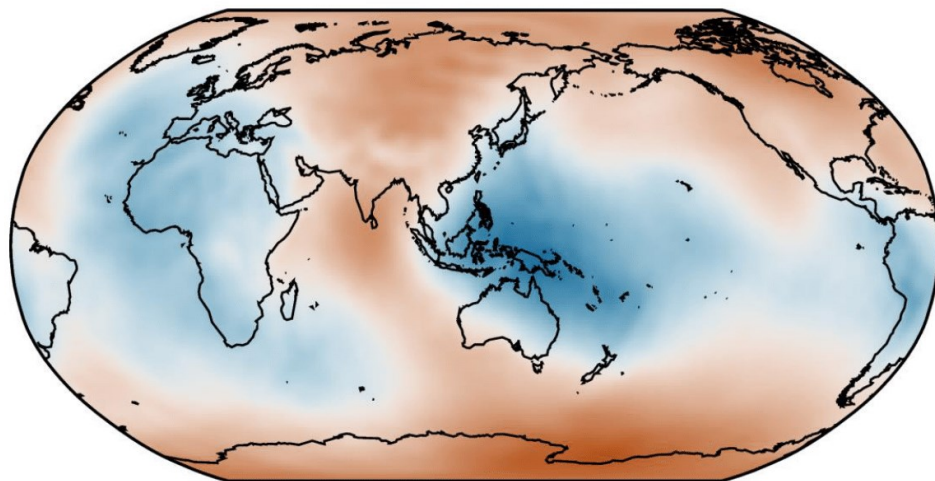


Figure 3.21 Modeled geoid map for Case 3. The correlation (fit) is 0.74.



## CHAPTER 4. DISCUSSION

### 4.1 Reliability analysis of inferred global mantle discontinuities

Spectrum amplitude charts (Figures 3.1–3.3) and cluster center charts (Figures 3.7–3.9) show that it is adequate to extract seismic models (Models S362WMANI+M, SEMUCB-WM1, and S40RTS) up to degree 60. Cluster center charts also demonstrate the consistency of clusters over depth and degree ranges. By comparing global cluster maps to global shear velocity variation maps (see Figures 3.4–3.6), the accuracy of clusters is validated. By comparing the heterogeneity percentage profiles at the chosen low degree and degree 60 for each model (see Figure 3.13–3.15), we can confirm that all seismic models become stable before degree 60. In conclusion, it is appropriate to use heterogeneity percentage profiles at degree 60 in this research.

Heterogeneity percentage profiles, as confirmed in Figures 3.10 and 3.11, are independent of the reference model and data type. As shown in Figure 3.12, it is meaningless to compare cluster percentages directly. However, abrupt shifts in heterogeneity percentage profiles have geophysical significance. They can be compared among seismic models. The reduced depth resolution has no effect on the recognition of key cluster percentage shifts (see Figures 3.16–3.18). By using profiles from three distinct seismic models, the bias from a specific model is avoided. All in all, global mantle discontinuities inferred from key cluster percentage shifts in heterogeneity percentage profiles at degree 60, as displayed in Figures 3.16–3.18, are reliable.

### 4.2 Global discontinuities in the mantle

Global mantle discontinuities around 400 km, 650 km, 1050 km, 1500 km, and 2700 km are deduced from heterogeneity percentage profiles at degree 60 (Figures 3.16–

3.18). Among all five discontinuities, 400 km, 650 km, and 2700 km discontinuities are generally acknowledged by scholars.

#### 4.2.1 400 km, 650 km, and 2700 km discontinuities

There are scientific reports of seismic discontinuities at around 400 km and 650 km deep beneath different regions (e.g., Niazi & Anderson, 1965; Richards & Wicks Jr, 1990; Simmons & Gurrola, 2000; Ai & Zheng, 2003). These two discontinuities are also included in the global model PREM. In heterogeneity percentage profiles (Figure 3.16–3.18), key cluster percentage shifts related to the discontinuities are noticeable.

Located at the lowermost mantle, the D'' layer is characterized by seismic stratification (van der Hilst, et al., 2007). A key cluster percentage shift around 2700 km is recognized in all three heterogeneity percentage profiles (Figure 3.16–3.18). The indicated 2700 km global discontinuity coincides with the predicted location of a solid-solid mineral phase transition (Sidorin, Gurnis, & Helmberger, 1999). D'' discontinuity at around 250–270 km above CMB (Wyssession, et al., 1998; He & Wen, 2011), whose correlated cluster percentage shift is only observed in the profile for Model S40RTS (Figure 3.14) at around 2600 km, is likely a regional discontinuity.

#### 4.2.2 1050 km and 1500 km discontinuities

The “920 km discontinuity” is observed under subduction regions and regarded as a global discontinuity, with its depth varying between 900 km and 1080 km (Kawakatsu & Niu, 1994; Niu & Kawakatsu, 1997; Vinnik, Kato, & Kawakatsu, 2001; Vanacore, Niu, & Kawakatsu, 2006). However, cluster percentage shifts at approximately 900 km and 1050 km can be detected in all three heterogeneity percentage profiles (Figure 3.13–3.15). They indicate the existence of two separate discontinuities. Since the 900 km shift is

inconspicuous in the profiles for Models S362ANI+M and S40RTS (Figure 3.13 and Figure 3.14), it is possible that the "920 km discontinuity" is a local discontinuity beneath certain subduction regions. The reported large depth variation of this discontinuity is most likely the result of confusing the 900 km discontinuity with the 1050 km discontinuity.

The 1050 km shift, unlike the 900 km shift, is a key cluster percentage shift observed in all three heterogeneity percentage profiles. It indicates a global discontinuity in the mantle. In addition to subduction regions, this discontinuity is also observed beneath non-subduction regions (Shen, Wolfe, & Solomon, 2003; Courtier, Bagley, & Revenaugh, 2007; Jenkins, Deuss, & Cottaar, 2017; Zhang, Irving, Simons, & Alkhalifah, 2023). The velocity spectrum of Model SESGLOB2 (a mantle tomographic model not used in this study) changes markedly at around 1000 km (Durand, Debayle, Ricard, Zanolli, & Lambotte, 2017). It also implies that the 1050 km discontinuity is a global discontinuity.

Similar to the 1050 km discontinuity, the 1500 km global discontinuity is inferred from the key cluster percentage shift at around 1500 km. This discontinuity has also been suggested by other seismic studies. In the depth profile of parameter ( $d \ln V_s / d \ln V_p$ ), values for slab and non-slab regions differ considerably below 1500 km depth (Saltzer, van der Hilst, & Kárason, 2001). The ratio ( $d \ln \rho / d \ln V_s$ ) reaches a maximum at about 1500 km depth in research with degree 2 splitting coefficients (Romanowicz, 2001). In the analysis of shear velocity anomalies in tomographic models, the transition of domination between slow and fast anomalies is observed at around 1500 km depth (Houser & Williams, 2009). There are scientific reports about spin transitions of iron in lower mantle minerals (Badro, et al., 2004; Lin, et al., 2007). The spin transition zone is centered at approximately 1500 km (Garnero & McNamara, 2008).

### 4.3 Transition zones in the mantle

#### 4.3.1 Upper mantle transition zone (UMTZ)

After discovering global discontinuities at depths around 400 and 650 km, respectively, the upper mantle transition zone (UMTZ), which is constrained by these two discontinuities, has been intensively investigated by different researchers (e.g., Dueker & Sheehan, 1997; Gurrola & Minster, 1998; Gu & Dziewonski, 2002; Schmerr & Garnero, 2006; Burky, Irving, & Simons, 2023). Two key cluster percentage shifts, located at around 400 and 650 km depth, are identified in all heterogeneity percentage profiles (Figures 3.16–3.18). Therefore, the depth range of UMTZ is limited to between 400 km and 650 km in this study.

#### 4.3.2 Middle mantle transition zone (MMTZ)

Two key cluster percentage shifts at around 1050 and 1500 km are noticeable in all heterogeneity percentage profiles (Figures 3.16–3.18). There are two global discontinuities at corresponding depths, as indicated by these two shifts. The region bounded by these two discontinuities represents a new transition zone in the middle mantle. The middle mantle transition zone (MMTZ) was predicted by Dziewonski in 1977. Due to the unreliability of partial results, its upper boundary was set at 1100 km depth (Dziewonski, Hager, & O'Connell, 1977). In this research, after identifying these two global discontinuities together, the MMTZ is discovered for the first time. Accordingly, its depth range is determined to be between 1050 km and 1500 km.

### 4.4 Viscosity jump in MMTZ and its geodynamical significance

By using a Bayesian method to infer the mantle's viscosity structure, a viscosity jump at around 1000 km depth, near the upper boundary of MMTZ, is detected (Rudolph,

Lekić, & Lithgow-Bertelloni, 2015; Rudolph, Moulik, & Lekić, 2020). As shown in Table 3.1 and Figures 3.19–3.21, increasing the viscosity ratio of the layer between 1000 km and 1500 km significantly improves the correlation between the modeled geoid and the global geoid observation. This indicates a viscosity jump in MMTZ.

For mantle dynamics, the viscosity jump in MMTZ is critical. It explains the seismic observations of the most significant components, the subduction slab and mantle plume, in the deep mantle. For example, the trunk of Indo-Austral mantle plumes splits at around 1500 km and 1000 km (Tsekhmistrenko, Sigloch, Hosseini, & Barruol, 2021). In the four stages of slab descent beneath major subduction zones around the circum-Pacific, the slab is trapped above 1000 km in stage three (Fukao & Obayashi, 2013).

## CHAPTER 5. CONCLUSION

Seismic tomography has been extensively used to explore the mantle's structure. In this research, we apply K-Means clustering to shear velocity variation data from three different seismic models and synthesize their heterogeneity percentage profiles. Global mantle discontinuities are inferred from key cluster percentage shifts in profiles. Then, we perform mantle convection modeling to investigate the possible viscosity jump associated with discontinuities of interest.

Key cluster percentage shifts correlated to acknowledged global discontinuities (400 km, 650 km, and 2700 km discontinuities) are observed in all heterogeneity percentage profiles. The 1050 km discontinuity previously reported is now confirmed to be a global discontinuity. Research results also suggest the existence of two new global discontinuities: a 1500 km discontinuity and a lower mantle discontinuity between 2200 km and 2600 km. Geodynamic modeling with the global geoid indicates that there is a viscosity jump in the depth range of 1000–1500 km. This viscosity jump explains the seismic observations of subduction slabs and mantle plumes.

In conclusion, we discovered the middle mantle transition zone (MMTZ). It is bounded between two global discontinuities at depths of 1050 km and 1500 km. In addition, we show a viscosity jump of a factor of 10 to 30 in this new transition zone.

## REFERENCES

- Ai, Y., & Zheng, T. (2003). The upper mantle discontinuity structure beneath eastern China. *Geophysical Research Letters*.
- Badro, J., Rueff, J., Vankó, G., Monaco, G., Fiquet, G., & Guyot, F. (2004). Electronic Transitions in Perovskite: Possible Nonconvecting Layers in the Lower Mantle. *Science*.
- Bergen, K. J., Johnson, P. A., de Hoop, M. V., & Beroza, G. C. (2019). Machine learning for data-driven discovery in solid Earth geoscience. *Science*.
- Burky, A. L., Irving, J. C., & Simons, F. J. (2023). The mantle transition zone beneath eastern North America: Receiver functions and tomographic velocity models. *Physics of the Earth and Planetary Interiors*.
- Cottaar, S., & Deuss, A. (2016). Large-scale mantle discontinuity topography beneath Europe: Signature of akimotoite in subducting slabs. *Journal of Geophysical Research: Solid Earth*.
- Cottaar, S., & Lekic, V. (2016). Morphology of seismically slow lower-mantle structures. *Geophysical Journal International*.
- Courtier, A. M., Bagley, B., & Revenaugh, J. (2007). Whole mantle discontinuity structure beneath Hawaii. *Geophysical Research Letters*.
- Davies, C. J., Stegman, D. R., & Dumberry, M. (2014). The strength of gravitational core-mantle coupling. *Geophysical Research Letters*.
- Davies, D. R., Valentine, A. P., Kramer, S. C., Rawlinson, N., Hoggard, M. J., Eakin, C. M., & Wilson, C. R. (2019). Earth's multi-scale topographic response to global mantle flow. *Nature Geoscience*.
- Dietz, R. S. (1961). Continent and ocean basin evolution by spreading of the sea floor. *Nature*.
- Dueker, K. G., & Sheehan, A. F. (1997). Mantle discontinuity structure from midpoint stacks of converted P to S waves across the Yellowstone hotspot track. *Journal of Geophysical Research: Solid Earth*.
- Durand, S., Abreu, R., & Thomas, C. (2018). SeisTomoPy: Fast Visualization, Comparison, and Calculations in Global Tomographic Models. *Seismological Research Letters*.
- Durand, S., Debayle, E., Ricard, Y., Zaroли, C., & Lambotte, S. (2017). Confirmation of a change in the global shear velocity pattern at around 1000 km depth. *Geophysical Journal International*.

- Dziewonski, A. M., & Anderson, D. L. (1981). Preliminary reference Earth model. *Physics of the earth and planetary interiors*.
- Dziewonski, A. M., Hager, B. H., & O'Connell, R. J. (1977). Large-scale heterogeneities in the lower mantle. *Journal of Geophysical Research*.
- Fiquet, G., Dewaele, A., Andrault, D., Kunz, M., & Le Bihan, T. (2000). Thermoelastic properties and crystal structure of MgSiO<sub>3</sub> perovskite at lower mantle pressure and temperature conditions. *Geophysical Research Letters*.
- French, S. W., & Romanowicz, B. A. (2014). Whole-mantle radially anisotropic shear velocity structure from spectral-element waveform tomography. *Geophysical Journal International*.
- Fukao, Y., & Obayashi, M. (2013). Subducted slabs stagnant above, penetrating through, and trapped below the 660 km discontinuity. *Journal of Geophysical Research: Solid Earth*.
- Garnero, E. J., & McNamara, A. K. (2008). Structure and Dynamics of Earth's Lower Mantle. *Science*.
- Ghosh, A., Becker, T. W., & Zhong, S. J. (2010). Effects of lateral viscosity variations on the geoid. *Geophysical Research Letters*.
- Gu, Y. J., & Dziewonski, A. M. (2002). Global variability of transition zone thickness. *Journal of Geophysical Research: Solid Earth*.
- Gurrola, H., & Minster, J. B. (1998). Thickness estimates of the upper-mantle transition zone from bootstrapped velocity spectrum stacks of receiver functions. *Geophysical Journal International*.
- Hager, B. H., & O'Connell, R. J. (1981). A simple global model of plate dynamics and mantle convection. *Journal of Geophysical Research: Solid Earth*.
- Hager, B. H., & Richards, M. A. (1989). Long-wavelength variations in Earth's geoid: physical models and dynamical implications. *Philosophical Transactions of the Royal Society of London. Series A, Mathematical and Physical Sciences*.
- Hager, B. H., Clayton, R. W., Richards, M. A., Comer, R. P., & Dziewonski, A. M. (1985). Lower mantle heterogeneity, dynamic topography and the geoid. *Nature*.
- He, Y., & Wen, L. (2011). Seismic velocity structures and detailed features of the D "discontinuity near the core-mantle boundary beneath eastern Eurasia. *Physics of the Earth and Planetary Interiors*.
- Heister, T., Dannberg, J., Gassmüller, R., & Bangerth, W. (2017). High accuracy mantle convection simulation through modern numerical methods—II: realistic models and problems. *Geophysical Journal International*.



- Hess, H. H. (1962). History of Ocean Basins. In *Petrologic Studies*. Geological Society of America.
- Holmes, A. (1931). Radioactivity and Earth Movements. *Transactions of the Geological Society of Glasgow*.
- Houser, C., & Williams, Q. (2009). The relative wavelengths of fast and slow velocity anomalies in the lower mantle: Contrary to the expectations of dynamics? *Physics of the Earth and Planetary Interiors*.
- Houser, C., Masters, G., Shearer, P., & Laske, G. (2008). Shear and compressional velocity models of the mantle from cluster analysis of long-period waveforms. *Geophysical Journal International*.
- Iitaka, T., Hirose, K., Kawamura, K., & Murakami, M. (2004). The elasticity of the MgSiO<sub>3</sub> post-perovskite phase in the Earth's lowermost mantle. *Nature*.
- Irifune, T., & Tsuchiya, T. (2015). Phase Transitions and Mineralogy of the Lower Mantle. In *Treatise on Geophysics (Second Edition)*. Elsevier.
- Jenkins, J., Deuss, A., & Cottaar, S. (2017). Converted phases from sharp 1000 km depth mid-mantle heterogeneity beneath Western Europe. *Earth and Planetary Science Letters*.
- Kawakatsu, H., & Niu, F. (1994). Seismic evidence for a 920-km discontinuity in the mantle. *Nature*.
- Kronbichler, M., Heister, T., & Bangerth, W. (2012). High accuracy mantle convection simulation through modern numerical methods. *Geophysical Journal International*.
- Le Pichon, X. (1968). Sea-floor spreading and continental drift. *Journal of geophysical research*.
- Lekic, V., & Romanowicz, B. (2011). Tectonic regionalization without a priori information: A cluster analysis of upper mantle tomography. *Earth and Planetary Science Letters*.
- Lekic, V., Cottaar, S., Dziewonski, A., & Romanowicz, B. (2012). Cluster analysis of global lower mantle tomography: A new class of structure and implications for chemical heterogeneity. *Earth and Planetary Science Letters*.
- Li, Y., Wang, H., Li, Y., Ye, H., Zhang, Y., Yin, R., . . . Lu, A. (2023). Electron transfer rules of minerals under pressure informed by machine learning. *Nature Communications*.
- Lin, J., Vankó, G., Jacobsen, S. D., Iota, V., Struzhkin, V. V., Prakapenka, V. B., . . . Yoo, C. (2007). Spin Transition Zone in Earth's Lower Mantle. *Science*.

- Liu, X., & Zhong, S. (2015). The long-wavelength geoid from three-dimensional spherical models of thermal and thermochemical mantle convection. *Journal of Geophysical Research: Solid Earth*.
- Liu, X., & Zhong, S. (2016). Constraining mantle viscosity structure for a thermochemical mantle using the geoid observation. *Geochemistry, Geophysics, Geosystems*.
- Mao, W., & Zhong, S. (2018). Slab stagnation due to a reduced viscosity layer beneath the mantle transition zone. *Nature Geoscience*.
- Morgan, W. J. (1971). Convection plumes in the lower mantle. *Nature*.
- Morgan, W. J. (1972). Plate motions and deep mantle convection. *Geological Society of America Memoirs*.
- Moucha, R., Forte, A. M., Mitrovica, J. X., & Daradich, A. (2007). Lateral variations in mantle rheology: implications for convection related surface observables and inferred viscosity models. *Geophysical Journal International*.
- Moulik, P., & Ekström, G. (2014). An anisotropic shear velocity model of the Earth's mantle using normal modes, body waves, surface waves and long-period waveforms. *Geophysical Journal International*.
- Murakami, M., Hirose, K., Kawamura, K., Sata, N., & Ohishi, Y. (2004). Post-perovskite phase transition in MgSiO<sub>3</sub>. *Science*.
- Niazi, M., & Anderson, D. L. (1965). Upper mantle structure of western North America from apparent velocities of P waves. *Journal of Geophysical Research*.
- Niu, F., & Kawakatsu, H. (1997). Depth variation of the mid-mantle seismic discontinuity. *Geophysical Research Letters*.
- Pavlis, N. K., Holmes, S. A., Kenyon, S. C., & Factor, J. K. (2012). The development and evaluation of the Earth Gravitational Model 2008 (EGM2008). *Journal of Geophysical Research: Solid Earth*.
- Ricard, Y., Richards, M., Lithgow-Bertelloni, C., & Le Stunff, Y. (1993). A geodynamic model of mantle density heterogeneity. *Journal of Geophysical Research: Solid Earth*.
- Richards, M. A., & Hager, B. H. (1984). Geoid anomalies in a dynamic Earth. *Journal of Geophysical Research: Solid Earth*.
- Richards, M. A., & Hager, B. H. (1989). Effects of lateral viscosity variations on long-wavelength geoid anomalies and topography. *Journal of Geophysical Research: Solid Earth*.

- Richards, M. A., & Wicks Jr, C. W. (1990). S–P conversions from the transition zone beneath Tonga and the nature of the 670 km discontinuity. *Geophysical Journal International*.
- Ringwood, A. E. (1969). Phase transformations in the mantle. *Earth and Planetary Science Letters*.
- Ritsema, J., Deuss, A., van Heijst, H. J., & Woodhouse, J. H. (2011). S40RTS: a degree-40 shear-velocity model for the mantle from new Rayleigh wave dispersion, teleseismic traveltime and normal-mode splitting function measurements. *Geophysical Journal International*.
- Romanowicz, B. (2001). Can we resolve 3D density heterogeneity in the lower mantle? *Geophysical Research Letters*.
- Rouet-Leduc, B., Hulbert, C., Lubbers, N., Barros, K., Humphreys, C. J., & Johnson, P. A. (2017). Machine learning predicts laboratory earthquakes. *Geophysical Research Letters*.
- Rudolph, M. L., Lekić, V., & Lithgow-Bertelloni, C. (2015). Viscosity jump in Earth's mid-mantle. *Science*.
- Rudolph, M. L., Moulik, P., & Lekić, V. (2020). Bayesian inference of mantle viscosity from whole-mantle density models. *Geochemistry, Geophysics, Geosystems*.
- Saltzer, R. L., van der Hilst, R. D., & Káráson, H. (2001). Comparing P and S wave heterogeneity in the mantle. *Geophysical Research Letters*.
- Schmerr, N., & Garnero, E. (2006). Investigation of upper mantle discontinuity structure beneath the central Pacific using SS precursors. *Journal of Geophysical Research: Solid Earth*.
- Schmerr, N., & Garnero, E. J. (2007). Upper mantle discontinuity topography from thermal and chemical heterogeneity. *Science*.
- Shen, Y., Wolfe, C. J., & Solomon, S. C. (2003). Seismological evidence for a mid-mantle discontinuity beneath Hawaii and Iceland. *Earth and Planetary Science Letters*.
- Shim, S. H., Duffy, T. S., & Shen, G. (2000). The stability and P–V–T equation of state of CaSiO<sub>3</sub> perovskite in the Earth's lower mantle. *Journal of Geophysical Research: Solid Earth*.
- Shim, S. H., Duffy, T. S., & Shen, G. (2001). The post-spinel transformation in Mg<sub>2</sub>SiO<sub>4</sub> and its relation to the 660-km seismic discontinuity. *Nature*.
- Sidorin, I., Gurnis, M., & Helmberger, D. V. (1999). Evidence for a Ubiquitous Seismic Discontinuity at the Base of the Mantle. *Science*.

- Simmons, N. A., & Gurrola, H. (2000). Multiple seismic discontinuities near the base of the transition zone in the Earth's mantle. *Nature*.
- Stadler, G., Gurnis, M., Burstedde, C., Wilcox, L. C., Alisic, L., & Ghattas, O. (2010). The dynamics of plate tectonics and mantle flow: From local to global scales. *Science*.
- Su, W. J., Woodward, R. L., & Dziewonski, A. M. (1994). Degree 12 model of shear velocity heterogeneity in the mantle. *Journal of Geophysical Research: Solid Earth*.
- Tackley, P. J. (2008). Modelling compressible mantle convection with large viscosity contrasts in a three-dimensional spherical shell using the yin-yang grid. *Physics of the Earth and Planetary Interiors*.
- Thoraval, C., & Richards, M. A. (1997). The geoid constraint in global geodynamics: viscosity structure, mantle heterogeneity models and boundary conditions. *Geophysical Journal International*.
- Tsekhmistrenko, M., Sigloch, K., Hosseini, K., & Barruol, G. (2021). A tree of Indo-African mantle plumes imaged by seismic tomography. *Nature Geoscience*.
- Turcotte, D. L. (1967). Finite amplitude convective cells and continental drift. *Journal of Fluid Mechanics*.
- van der Hilst, R. D., de Hoop, M. V., P., W., Shim, S. \_, P., M., & L., T. (2007). Seismostratigraphy and Thermal Structure of Earth's Core-Mantle Boundary Region. *Science*.
- Vanacore, E., Niu, F., & Kawakatsu, H. (2006). Observations of the mid-mantle discontinuity beneath Indonesia from S to P converted waveforms. *Geophysical Research Letters*.
- Vinnik, L., Kato, M., & Kawakatsu, H. (2001). Search for seismic discontinuities in the lower mantle. *Geophysical Journal International*.
- Wang, X., Holt, W. E., & Ghosh, A. (2015). Joint modeling of lithosphere and mantle dynamics: Evaluation of constraints from global tomography models. *Journal of Geophysical Research: Solid Earth*.
- Wegener, A. (1966). *The origin of continents and oceans*. Courier Corporation.
- Wilson, J. T. (1963). A possible origin of the Hawaiian Islands. *Canadian Journal of Physics*.
- Wilson, J. T. (1963). Continental drift. *Scientific American*.
- Wilson, J. T. (1965). Evidence from ocean islands suggesting movement in the Earth. *Philosophical Transactions of the Royal Society of London. Series A, Mathematical and Physical Sciences*.

- Wu, W., Ni, S., & Irving, J. C. (2019). Inferring Earth's discontinuous chemical layering from the 660-kilometer boundary topography. *Science*.
- Wysession, M. E., Lay, T., Revenaugh, J., Williams, Q., Garnero, E. J., Jeanloz, R., & Kellogg, L. H. (1998). The D "discontinuity and its implications. In *The core-mantle boundary region*. American Geophysical Union.
- Zeng, L., Sasselov, D. D., & Jacobsen, S. B. (2016). Mass–radius relation for rocky planets based on PREM. *The Astrophysical Journal*.
- Zhang, Z., Irving, J. C., Simons, F. J., & Alkhalifah, T. (2023). Seismic evidence for a 1000 km mantle discontinuity under the Pacific. *Nature communications*.
- Zhong, S., & Davies, G. F. (1999). Effects of plate and slab viscosities on the geoid. *Earth and Planetary Science Letters*.
- Zhong, S., Zuber, M. T., Moresi, L., & Gurnis, M. (2000). Role of temperature-dependent viscosity and surface plates in spherical shell models of mantle convection. *Journal of Geophysical Research: Solid Earth*.

## VITA

Shocked by the destructive Sichuan earthquake in 2008, I decided to major in geology at the university. I graduated from Northwest University in 2015 with a bachelor's degree in science. In 2019, I took geophysical classes as a visiting student at the University of Alberta. At the University of Kentucky, I was offered the position of teaching assistant for around two years. During the pandemic, a special grant from the Institute of International Education was awarded to me to support my pursuit of this master's degree.

Yuping Wang